Laboratory physical modelling of block toppling instability by means of tilt tests

Engineering Geology

Laboratory physical modelling of block toppling instability by means of tilt tests

--Manuscript Draft--

Manuscript Number:	ENGEO_2020_1457R1
Article Type:	Research Paper
Keywords:	Block toppling; Physical model; 3D printing; Tilt test; 3DEC
Corresponding Author:	Ignacio Pérez-Rey Laboratorio de Geotecnia, CEDEX Madrid, Spain
First Author:	Ignacio Pérez-Rey
Order of Authors:	Ignacio Pérez-Rey
	Mauro Muñiz Menéndez
	Javier González
	Federico Vagnon
	Gabriel Walton
	Leandro R. Alejano
Abstract:	In this paper we present a physical modelling approach where the stability of rock blocks against toppling in the field can be estimated using a tilt table, engineered rock models and 3D-printed small-scale versions of a natural rock boulder. To achieve this goal, first, simple geometry rock elements are tilted and results interpreted according to analytical formulations. Then, more complex geometry engineered rock blocks, including some whose centers of gravity do not project on the center of the base element, are tested and results properly interpreted. Eventually, the 3D-printed version of the rock boulder is produced from 3D point clouds recovered in the field by means of a combination of photogrammetry and laser scanner techniques. Analytical formulations and numerical calculations have been used in order to validate the proposed approach, to explain the physical phenomena involved, and to allow for possible extension of the physical modelling results to different scenarios, such as those considering the influence of water or seismic loading on stability.
Suggested Reviewers:	Juan Ramon Vidal Romani juan.vidal.romani@udc.es
	Resat Ulusay resatulusay1987@gmail.com
	Andrea Segalini andrea.segalini@unipr.it
Response to Reviewers:	Dear Editor and Reviewers: On behalf of my co-authors, we kindly acknowledge all the illustrative and enriching comments on the original version of our manuscript. We have tried to implement all the corrections by following the comments and suggestions, as well as to polish the English usage of the entire manuscript. Please, find all the changes and comments in the 'Response Letter to Editor and Reviewers' attached to the re-submission of our manuscript. Sincerely, Dr. Ignacio Pérez-Rey (corresponding author) ignacio.perez@cedex.es

Response letter to Editor and Reviewers

Laboratory physical modelling of block toppling instability by means of tilt tests

Ignacio Pérez-Rey[a,*], Mauro Muñiz-Menéndez[a], Javier González[b], Federico Vagnon[c], Gabriel Walton[d], Leandro R. Alejano[e,d]

[a]*Laboratorio de Geotecnia, CEDEX, Madrid, Spain*

[b]*Departamento de Ingeniería Metalúrgica y Minas, Universidad Católica del Norte, Antofagasta, Chile*

[c]*Department of Earth Science, Università degli Studi di Torino, Torino, Italy*

[d]*Department of Geology and Engineering Geology, Colorado School of Mines, Golden, USA*

[e]*Department of Natural Resources and Environmental Engineering, University of Vigo, Vigo, Spain*

[*]*corresponding author: ignacio.perez@cedex.es*

NOTE: In the following, we present the 'letter of reply' to the questions raised by the Editor and Reviewers regarding our article *Laboratory physical modelling of block toppling instability by means of tilt tests*. The original text of the Editor and Reviewers has been kept in blue and our responses are presented in black. (Modifications to the original manuscript are presented in green in the corresponding updated version).

Editor and Reviewer comments:

Two reviewers found the manuscript to be of interest and already in a rather good shape. I concur.

Specifics

1) Language - please check again and polish. I noticed some problematic sentences (see on example below).

20 Then, more complex geometry engineered rock blocks, including some where its center of gravity does not project on the center of the base element, are tested and results properly interpreted." - please improve English; for example, "some where its center of gravity does not" shoud probably read: some whose centers of gravity do not

2) Figures - 23 is a lot and I wonder if you really need all of them; perhaps some could be combined?

3) Highlights - please add (see Journal's Guide for Authors)

Authors

Dear Editor:

First, we would like to acknowledge the positive general assessment of the manuscript. Additionally, we thank you and both reviewers for all the comments on our manuscript, since they will ultimately contribute to the improvement of our work.

Regarding your specific comments and suggestions:

1) English usage has been polished again and some sentences were re-written by considering also those language corrections proposed by **Reviewer #2**. These sentences are indicated in the new version of the manuscript in green color.

2) Some Figures were combined into one so as to reduce its total number (now 20 instead of 23), as proposed. Figures combined were: (Fig. 12 + Fig. 13) now **Fig. 13**, (Fig. 16 + Fig. 17) now **Fig. 16**, (Fig. 18 + Fig. 19) now **Fig. 17**, (Fig. 21 + Fig. 22) now **Fig. 19**. A new figure was included following a reviewer's suggestion and Fig. 19 has been slightly modified for better understanding.

3) The 'Highlights' have been included according to the Journal's Guide of Authors in the new Submission process in a separate document.

Reviewer #1:

The paper presents an interesting study and is clearly presented, well written and easy to read. On my personal opinion it can be published as it is, without further revisions.

Authors

Dear Reviewer #1:

We kindly acknowledge these positive comments and the opinion regarding our paper. Thanks.

Reviewer #2 (R#2):

Corrections, comments, suggestions in the attached file.

Authors

Dear Reviewer #2:

We kindly acknowledge all the comments and suggestions. We thank you for the enriching comments and we tend to agree with all the suggested modifications, which have been implemented in the new version of the manuscript and indicated in green.

R#2 (comment made by R#2 referred to Eq. 3 in the original version of our manuscript)

It is a "correction", but an extension. Fig 3 is derived from static equations only, and it is not incorrect. Sagaseta extended the graph considering the dynamic equations. His graph should be included here, after equation (3) with a suitable explanation.

Authors

Thanks for this suggestion. In order to clarify this issue, a new Figure (Fig. 4) containing the boundary conditions for toppling, as published by Sagaseta (1986) has been embedded in the new version of the manuscript. The chart has been remade based on the equations established by Sagaseta (1986) for dynamic conditions, as presented in our paper, and it is included with a suitable explanation, as requested by R#2, after Eq. 3 in the way shown below:

If Eq. 3 is considered, the boundary conditions for the possible modes of failure for a slab-like straight block with slenderness b/h, placed on an inclined plane dipping α degrees and with a friction angle $\phi = 30^{o}$ can be correctly plotted (Fig. 4).

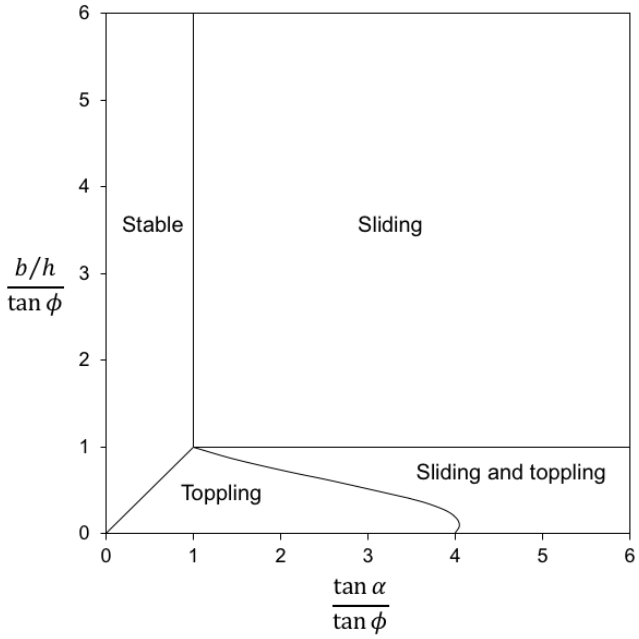

Fig. 4 Stability chart for dynamic conditions, considering a block of dimensions $b \times h$ placed on a inclined plane dipping α degrees (as modified from Sagaseta (1986)). The line dividing toppling and sliding + toppling failure regions corresponds to a friction angle $\phi = 30^{o}$.

For a block such as the already referred, in Fig. 4 the stability region is determined by the vertical line ($\tan \alpha = \tan \phi$) and the 1:1 line ($\tan \alpha = b/h$). The sliding failure will take place for the region defined by the same vertical line and the condition $\tan \phi = b/h$ (horizontal line). The curved line, as derived from Eq. 3, divides the toppling and toppling + sliding failure regions. Note that the position of this line will depend on the friction angle, and will always intercept the horizontal axis at a value $\tan \alpha = 4 \cdot \tan \phi$.

R#2 (comment made by R#2 referred to Eq. 22 in the original version of our manuscript)

Why not display the equation for alfacrit as a function of a and b, as in PM-2?

Authors

Thanks for this comment. We find this suggestion appropriate, and we have added a short paragraph with a new equation relating the stabilizing and overturning (toppling) moments as a function of *a* and *b* (as in PM-2). The new text and Equation are provided below, as included in the new (corrected) version of the manuscript:

In a similar way as presented in Eq. 8, the angle of critical toppling can also be estimated as a function of *a* and *b* dimensions of the specimen (Eq. 23):

$$\alpha_{cr} = \operatorname{atan}\left[\frac{(W_1 + W_2)\frac{b}{2}}{W_1 \cdot a + W_2 \cdot \frac{3a}{2}}\right] \tag{23}$$

Laboratory physical modelling of block toppling instability by means of tilt tests

Ignacio Pérez-Rey[a,*], Mauro Muñiz-Menéndez[a], Javier González[b], Federico Vagnon[c], Gabriel Walton[d], Leandro R. Alejano[e,d]

[a]*Laboratorio de Geotecnia, CEDEX, Madrid, Spain*

[b]*Departamento de Ingeniería Metalúrgica y Minas, Universidad Católica del Norte, Antofagasta, Chile*

[c]*Department of Earth Science, Università degli Studi di Torino, Torino, Italy*

[d]*Department of Geology and Engineering Geology, Colorado School of Mines, Golden, USA*

[e]*Department of Natural Resources and Environmental Engineering, University of Vigo, Vigo, Spain*

[*]*corresponding author: ignacio.perez@cedex.es*

ABSTRACT

In this paper we present a physical modelling approach where the stability of rock blocks against toppling in the field can be estimated using a tilt table, engineered rock models and 3D-printed small-scale versions of a natural rock boulder. To achieve this goal, first, simple geometry rock elements are tilted and results interpreted according to analytical formulations. Then, more complex geometry engineered rock blocks, including some whose centers of gravity do not project on the center of the base element, are tested and results properly interpreted. Eventually, the 3D-printed version of the rock boulder is produced from 3D point clouds recovered in the field by means of a combination of photogrammetry and laser scanner techniques. Analytical formulations and numerical calculations have been used in order to validate the proposed approach, to explain the physical phenomena involved, and to allow for possible extension of the physical modelling results to different scenarios, such as those considering the influence of water or seismic loading on stability.

List of symbols

α	base plane inclination angle
α_{cr}	critical angle of toppling
b	width of the block
cog	center of gravity
ϕ	friction angle
FS	factor of safety
g	acceleration of gravity (9.81 m/s^2)
h	height of the block or model
P	rotation pivot of a given block or model and origin of the (x_i, y_i) coordinates
r	radius
r_c	radius of the block corners (expressed as the radius of curvature)
x_i	distance from P to the cog of the i-th sub-section along the x-axis for a given block or model
y_i	distance from P to the cog of the i-th sub-section along the y-axis for a given block or model
w	width of the block (out of plane)
W	weight of the block
W_i	weight of the i-th section

1. Introduction

Analysing the stability of natural or man-made slopes in rock masses is a complex task. The principles of the discipline addressing this problem (typically known as rock slope engineering) were established in the seminal works developed during the 1960s and 1970s at Imperial College in London and by Richard Goodman in Berkeley, and they are summarized in the book entitled "Rock Slope Engineering" (Hoek and Bray, 1974). In this book, it was clearly stated that, unlike in the case of soils, where failure mechanisms typically involve sliding along a rotational or planar sliding surface, for rocks, a variety of failure mechanisms could occur according to the number, continuity, spacing, orientation and geomechanical characteristics of existing discontinuity sets.

Four typical types of failure mechanisms were identified at the time as the most common possibilities for rock slope instabilities: planar, wedge, (block) toppling and circular. This classification combined with the simple mathematical tools provided to analyse their stability, represented a significant step forward in the rock engineering field, leading to improved rock slope stability analyses and designs. However, as wisely noted in the preface of Hoek and Bray's (1974) book, 'Because the rock mass behind every slope is unique, there are no standard recipes or routine solutions which are guaranteed to produce the right answer each time they are applied'. This is why it is important to bear in mind that rock slope instability phenomena do not necessarily occur according to simple failure mechanisms as those described in these early works.

Whereas three of these basic mechanisms refer to sliding phenomena, only one of them involves toppling. Toppling corresponds to rotation of relatively slender rock columns or blocks about a fixed base. There are two distinct types of toppling failure mechanisms named block and flexural toppling (Goodman and Bray, 1976). In the first case, the toppling block is already fully detached from the rest of the rock mass. The second implies flexural or tensile failure, where the block is not completely detached of the rock mass such that new tensile failure cracks need to occur to fully detach the block from the surrounding ones for toppling instability to occur. In this study we focus on the analysis of block toppling.

The simplest toppling case considered in this study is that of a single toppling block. The first analyses of the stability against toppling of a single block were performed by Ashby (1971) and then extended and formalized by other authors (Hoek and Bray, 1974; Sagaseta, 1986). All these analyses start with strict geometrical assumptions considering perfectly rectangular blocks with sharp corners resting on a dipping plane striking in the same direction as the block face in contact with the plane.

Some studies have recently begun to address the influence of more realistic shapes of blocks on block stability against toppling. Alejano et al. (2015) studied the influence of the rounding of block corners on the stability of a block. This geometric condition observed in some rock masses and associated with spheroidal weathering erosive processes was shown to significantly affect block stability. The authors proposed a formulation to compute the stability of a round-cornered block to account for this effect. This formulation relies on the position of the potential rotation axis and was verified using physical models and field observations. While such a contribution is interesting and extends the type of toppling instability that can be analyzed, when one observes certain natural rock environments, more complex irregular block geometries exist for which no analysis methods can be observed.

As an example, Fig. 1 illustrates three zones in two different mountain environments, where a number of toppled and stable blocks are observed. In most of the cases and based on our current capabilities to analyze stability of blocks, it would be indeed difficult to rigorously perform a back analysis of the instability or stability of these blocks to explain why are they stable or unstable. For the stable blocks, it would also be difficult to assess their stability after a potential change in loading conditions, such as in the case of a seismic event. Accordingly, the main goal of this study is to develop a methodology through which the stability of complex blocks (such as those illustrated in Fig. 1) can be analyzed in a more or less reliable manner.

Since their early studies, the authors have considered cases involving increasingly complex estimates of the toppling stability of individual rock blocks taking into account the occurrence of rounded corners on the toppling blocks (Alejano et al., 2017) or rock boulders (Alejano et al., 2010b; Pérez-Rey et al., 2019). They also considered other studies available from literature focusing on the potential destabilizing effects of

earthquakes on rock blocks or groups of rock blocks (Christianson et al., 1995; Shi et al., 1996; Vann et al., 2019), where it has been necessary to extend available methodologies to model the nature of these structures in a more realistic manner.

In the process of developing the above-mentioned studies, tilting small-scale rock elements with simple geometries has revealed as an interesting technique that, in combination with analytical formulations can help to understand a number of issues associated to toppling phenomena. Therefore, a number of simple and a little bit more complex geometry engineered rock blocks have been tilted and results explained in this document to illustrate the potential interest of extending this technique to more realistic block shapes.

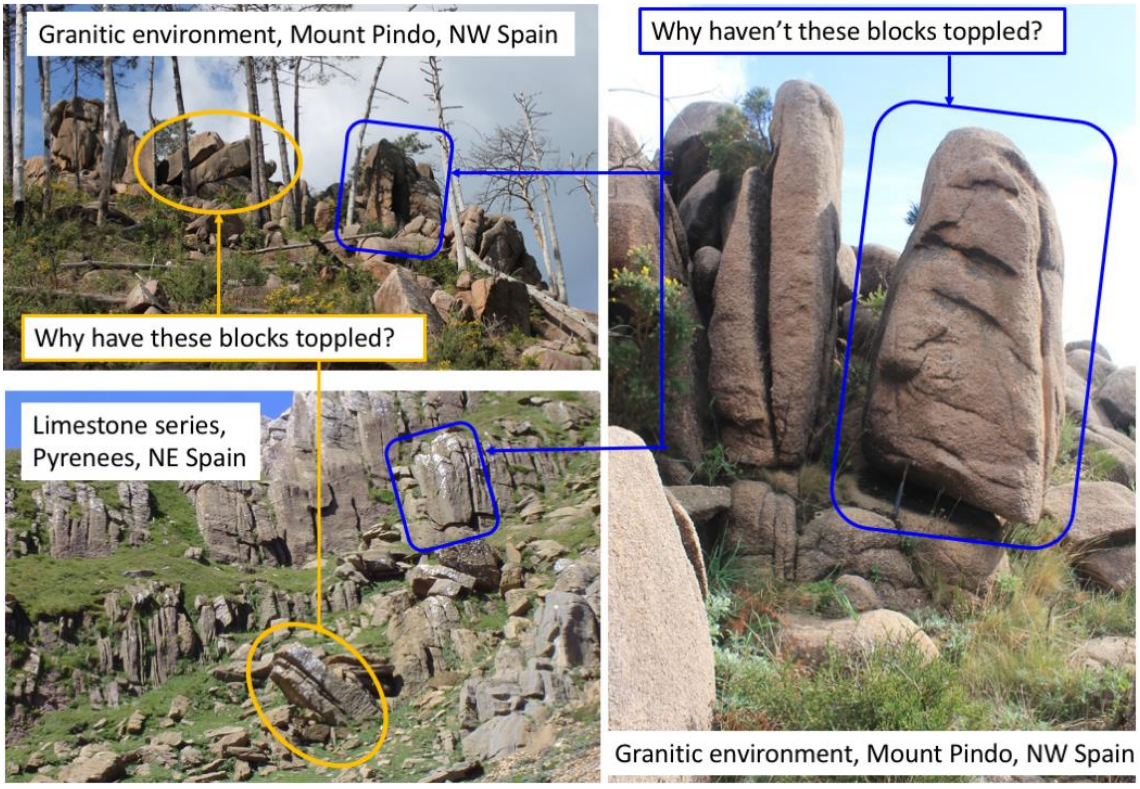

Fig. 1. Different geological environments where toppled and stable rock blocks are observed.

The study is an extension of basic toppling equilibrium calculations and was developed in parallel with particular rock slope stability studies. The initial concepts associated with the proposed methodology developed while studying the stability of footwall slopes (Alejano et al., 2011) and masonry retaining walls (Alejano et al., 2012). In both cases it was possible to resort to physical models subjected to tilt tests in order to carry out simple

analyses with the aim of confirming particular failure mechanisms and the validity of some formulations (Fig. 2). This previously developed approach is valid if only friction is involved, and block's geometries can be easily reproduced using common rock cutting approaches (typically with saw-blades).

Fig. 2. Physical models of dry masonry retaining walls used to understand the failure mechanism of these structures and check limit equilibrium calculations.

Since the turn of this century, photogrammetric and laser scanning techniques for point cloud acquisition have become widely available, such that a very good representation of a given rock slope geometry can be achieved (Alejano et al., 2013; Armesto et al., 2009; Ferrero et al., 2011, 2009; Riquelme et al., 2014). Most recently, relatively large and accurate 3D point clouds have become available at very reasonable costs (Girardeau-Montaut, 2018). It is therefore possible to obtain 3D point clouds representing the complex block geometries observed in nature (such as in Fig. 1). Based on such geometric data, the center of gravity (*cog*), which is critical for toppling stability analyses, can be precisely located. Other relevant geometrical aspects of the rock blocks or boulders such as the position of the contact base between the block and basal plane can be also rigorously defined. This geometrical information largely facilitates computing the factor of safety of these boulders against toppling, as the ratio of stabilizing moments to overturning moments.

Additionally, in the last five years, 3D printing has improved so rapidly that it is relatively easy to produce a scaled 3D printed version of any rock block based on the point cloud representing its outer surface (Bader et al., 2018; Virtanen et al., 2014). Therefore, it allows for the possibility of using tilt testing as a methodology to analyze the stability of blocks with complex geometry against toppling.

Consequently, in this paper we introduce a new physical modelling approach, where a tilt table, classic limit equilibrium computations, and rock physical models using a 3D-printed version of a real boulder are used to estimate the factor of safety against toppling of rock blocks in Nature. The use of analytical formulations and numerical models in parallel with this approach is strongly recommended. This would allow a deeper understanding of the phenomena at stake and will help to extend physical modelling observations to different scenarios (water pressure or dynamic loadings).

2. The mechanics of toppling

Despite the fact that some authors consider the occurrence of pure toppling as an uncommon failure mechanism, and that toppling is typically associated with larger failures or as a consequence of other mechanisms like slope undercutting or weakening at the toe (Hencher, 2015), toppling has been extensively reported as the origin of several rock-mass failures experienced in different fields such as open-pit mining (Al Mandalawi et al., 2019; Alejano et al., 2010a; Amini and Ardestani, 2019), civil engineering (Akbarpour et al., 2012; Cai et al., 2019; Tu et al., 2007) and natural rock slopes (Guo et al., 2017).

The mechanism of toppling had long been partially identified in the field by some authors (Müller, 1968; Terzaghi, 1962), though it was not until the late 1960's that it began to be considered as a mode of failure unto itself (Bray, 1969). A few years later, some authors started the study of toppling in a more rigorous way, through both laboratory models (Ashby, 1971; Barton, 1971) and early applications of numerical methods (Cundall, 1971; St. John, 1972).

Ashby (1971) developed a seminal study on different sliding and toppling modes of failure based on laboratory physical models and observations on rock slopes. This author derived a simplified analytical 2-D toppling model for an isolated straight block of height h and width b, resting on a plane dipping α degrees with a friction angle between contacts, ϕ (Fig. 3).

Considering the base plane angle, $\alpha < \phi$ and the *x* and *y* components of the weight (*W*) of the block, a factor of safety against toppling can be estimated by relating the stabilizing and overturning moments with respect to the rotation pivot, P (Fig. 3a), as presented in a general form in Eq. 1.

$$FS = \frac{\sum M_{stabilizing}}{\sum M_{overturning}} \quad (1)$$

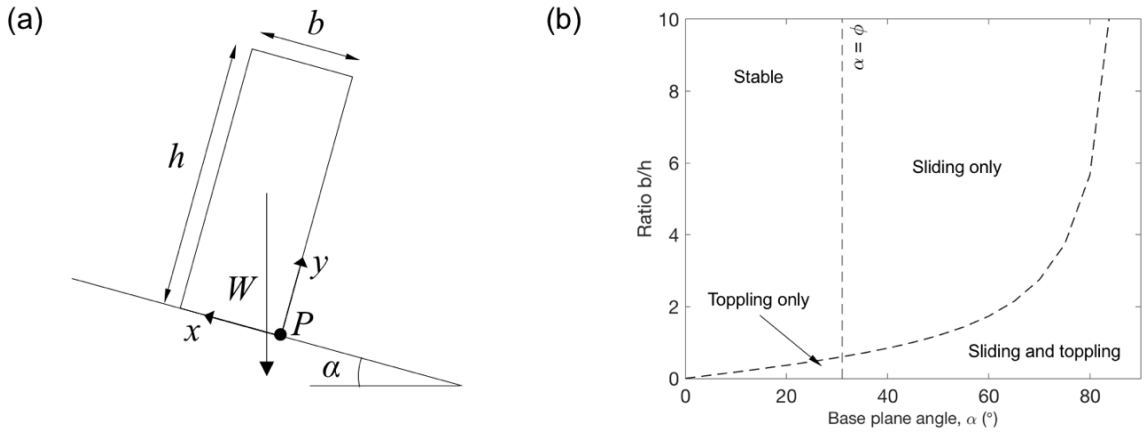

Fig. 3. (a) 2D sketch of a single block placed on an inclined plane for toppling stability analysis; (b) conditions for sliding and toppling according to Ashby (1971).

It is therefore easy to derive that the toppling condition (represented as FS ≤ 1 in Eq. 1) solely depends on the slenderness of the block and the plane dip (α) (Ashby, 1971) and is defined by the geometrical relationship presented in Eq. 2:

$$\frac{b}{h} \leq \tan \alpha \quad (2)$$

According to Fig. 3b and depending on the considered kinematic conditions stablished by Eq. 1 and the condition $\alpha = \phi$, that refers to sliding stability, four zones can be identified: stability, sliding, toppling and sliding and toppling simultaneously occurring. Even though this model laid the groundwork for subsequently reproduced studies on toppling (Hoek and Bray, 1974), some errors were detected in the conditions presented in Fig. 3b, as corrected by other authors (Bray and Goodman, 1981; Sagaseta, 1986). The

"corrected" solution for a single block toppling condition, as proposed by Sagaseta (1986), is given by Eq. 3:

$$\frac{4 \cdot \tan\alpha \cdot \left[1 + \left(\frac{b}{h}\right)^2\right] - 3 \cdot \left(\tan\alpha - \frac{b}{h}\right)}{4 \cdot \left[1 + \left(\frac{b}{h}\right)^2\right] + 3 \cdot \frac{b}{h} \cdot \left(\tan\alpha - \frac{b}{h}\right)} \leq \tan\phi \qquad (3)$$

If Eq. 3 is considered, the boundary conditions for the possible modes of failure for a slab-like straight block with slenderness b/h, placed on an inclined plane dipping α degrees and with a friction angle ϕ = 30º can be correctly plotted (Fig. 4).

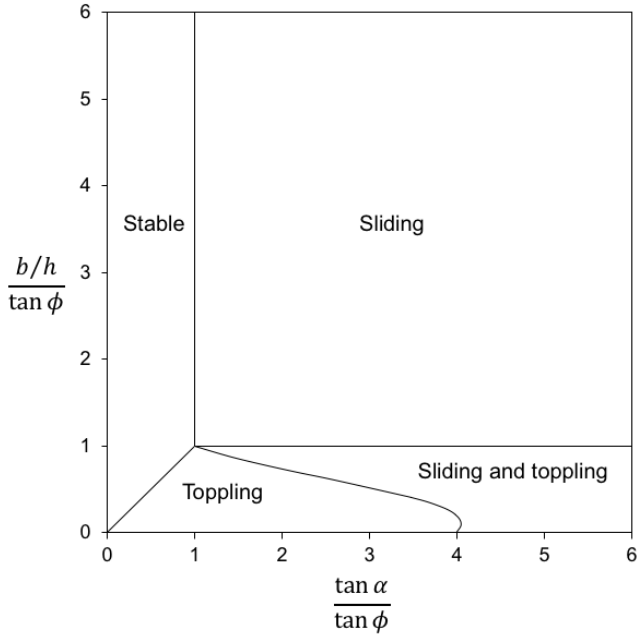

Fig. 4 Stability chart for dynamic conditions, considering a block of dimensions $b \times h$ placed on a inclined plane dipping α degrees (as modified from Sagaseta (1986)). The line dividing toppling and sliding + toppling failure regions corresponds to a friction angle ϕ = 30º.

For a block such as the already referred, in Fig. 4 the stability region is determined by the vertical line ($\tan\alpha = \tan\phi$) and the 1:1 line ($\tan\alpha = b/h$). The sliding failure will take place for the region defined by the same vertical line and the condition $\tan\phi = b/h$ (horizontal line). The curved line, as derived from Eq. 3, divides the toppling and toppling + sliding failure regions. Note that the position of this line will depend on the friction angle, and will always intercept the horizontal axis at a value $\tan\alpha = 4 \cdot \tan\phi$.

To consider the case of rounding on the block edges caused by weathering, the single 2D straight block model was reevaluated several years later (Alejano et al., 2015). Starting from Eq. 2, the authors proposed a new equation by considering a radius of curvature (r_c) representative of the edge rounding in such a way that toppling condition is given by the geometrical relationship presented in Eq. 4:

$$\frac{b - 2r_c}{h} < \tan \alpha \tag{4}$$

It must be noted that the approaches presented above should only be applied to 2D problems or to simplifications of 3D bodies presenting a constant cross-section, as illustrated in Fig. 5. Additionally, the rotating pivot is already known, and defined by an identifiable edge.

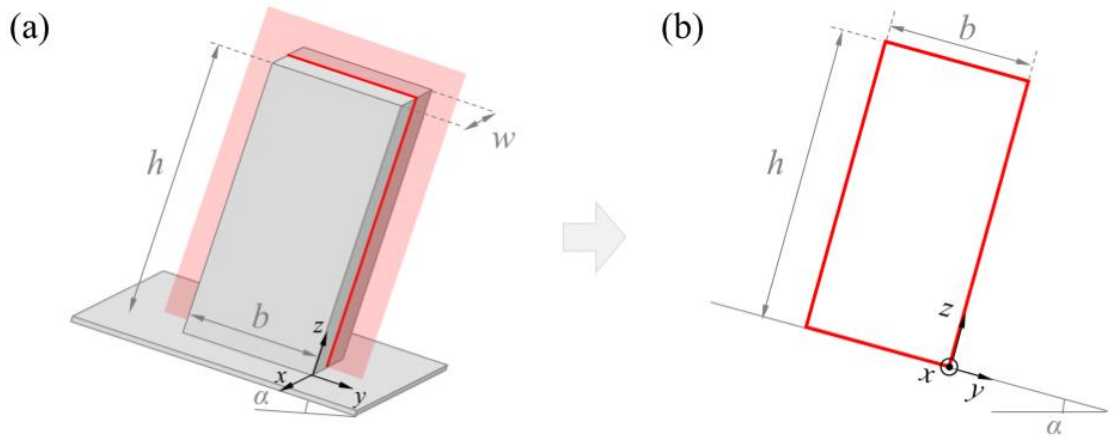

Fig. 5. (a) 3D body resting on an inclined plane with constant cross-section along the x-direction; (b) 2D simplification of the problem on the *z*–*y* plane.

Nevertheless, this situation is seldom found in natural blocks (particularly, in rock boulders), that usually present irregular shapes and poorly defined contact planes, such that 2D analyses are unrealistic. In these cases, the third dimension cannot be disregarded and other approaches are needed for a correct assessment of the toppling mechanism (Domokos et al., 2012; Yeung and Wong, 2007; Zábranová et al., 2020).

3. Analytical assessment and laboratory physical modelling

An experimental program was designed in order to study the critical angle of toppling of engineered models subjected to tilt tests under laboratory conditions. The idea was to test different blocks or assemblies presenting features that determine their kinematic behavior with respect to toppling: the symmetry of the block section, the edge rounding, the concavity of the contact base and the position of the center of gravity with respect to a central cross-section of the block. A sketch showing these features and the models used is presented in Fig. 6.

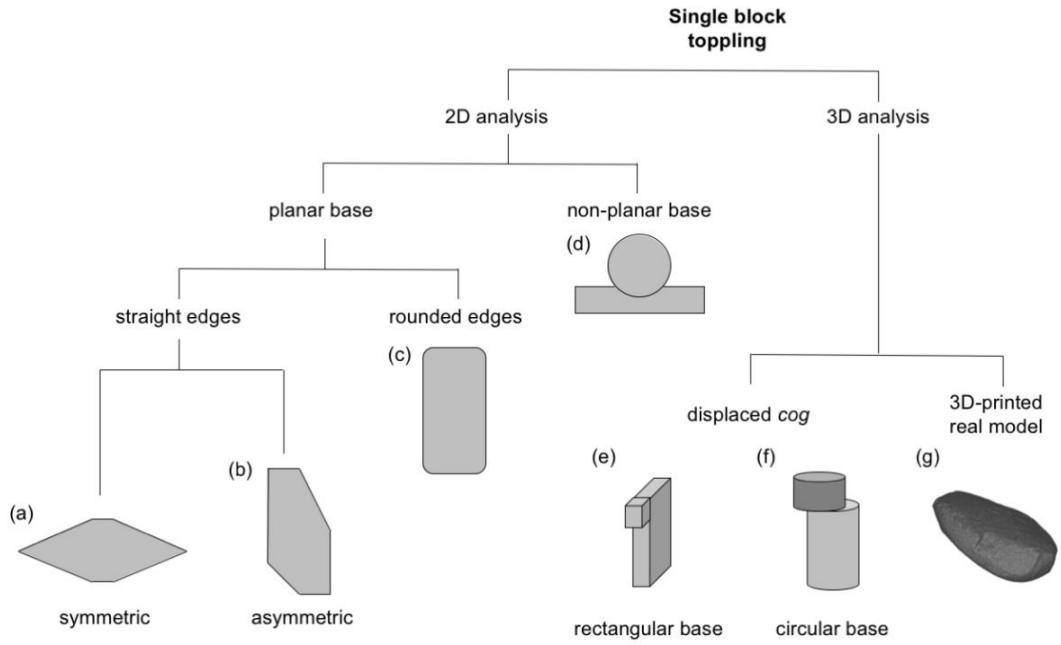

Fig. 6. Sketch showing the specimens used for 2D and 3D toppling analyses according to the type of contact base (planar or non-planar), edge rounding (straight or rounded), symmetry of the cross-section and position of the *cog*.

3.1. Physical models and laboratory testing

The models presented in Fig. 6 were selected to perform the laboratory tilt tests. The majority of them (Fig. 6 a–e) consisted of some saw-cut pieces of two igneous rocks (granite and orthogneiss) assembled by gluing them together to form the physical model (Fig. 7). A photo of each model is presented in Fig. 8. In mode case PM-6 (Fig. 6f and Fig. 8f), steel (with a density of 7900 kg/m^3) was used to fabricate the upper cylinder; as can be appreciated, this part of the model was intended to displace the center of gravity

of the corresponding assembly. The replica of a real boulder was 3D-printed with PLA (polylactide) plastic based on a 3D point cloud recovered from the original geological structure (Pérez-Rey et al., 2019).

The density of the plastic is lower than that of the rock. Additionally, the printed version presents an internal plastic pattern with regular hollow zones. Since toppling stability depends in both the stabilizing and overturning moments and they are both proportional to the block weight, density does not influence stability in uniform bodies. The friction force in the base is also proportional to the weight in case the contact is considered planar, though it may affect results for rough joints, as Barton's formula suggests. Since the contacts of the studied elements are typically planar, the weight does not significantly affect the frictional response. If one wants to avoid the sliding mechanism, in cases where it can take place at lower tilt angles than toppling, a piece of sand paper can be glued to the base of the element to increase friction strength. In conclusion, density, when constant, and friction angle are considered to have a negligible impact on the presented results.

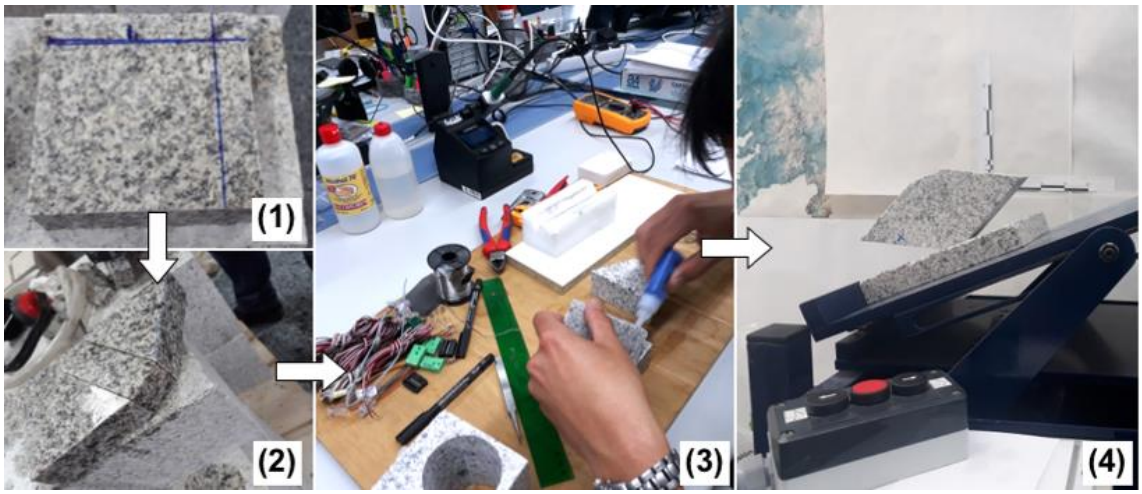

Fig. 7. Process of fabrication of the rock models (1, 2) dimensioning and parts of a model; (3) gluing of parts to create the complete model and (4) model being tested.

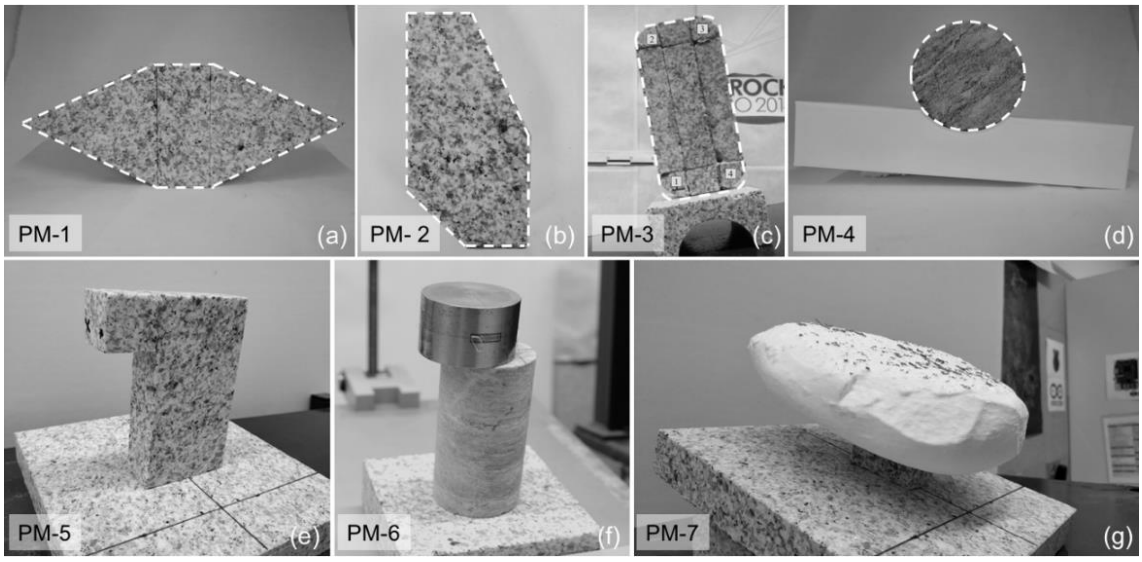

Fig. 8. Photos of the physical models used in this study (a. symmetric section; b. asymmetric section; c. rounded edges; d. concave base; e. displaced *cog* (rectangular base); f. displaced *cog* (circular base); g. 3D printed replica of a real boulder). The name assigned to each model is also provided.

Regarding the tilt tests, they were carried out with a testing frame designed at the University of Vigo that consists of a metallic platform able to rotate about a fixed axis and driven by an asynchronous motor that assures constant angular lifting velocities (from 0.1º/min to 26º/min) are maintained. The 'start' and 'stop' orders can be given to the machine by a manual control. A constant record of the tilting angle is kept using an inclinometer (*Leica DISTO D5*) with an accuracy of 0.1º attached to the platform (Fig. 9). The critical angle of toppling for each tested model could be registered by simply stopping the rotation of the platform as the onset of instability was observed. For that purpose, the tilting velocity was set at 12º/min for all tests in order to balance precision in determination of the critical angle with testing time. Each model was tested three times until toppling (or sliding, if it was the case) occurred, and results were collected for comparison with analytical and numerical predictions.

Fig. 9. Tilting platform used for carrying out tilt tests with the physical models (1. rotating platform; 2. connection box and velocity control; 3. 'start and stop' control; 4. digital inclinometer).

3.2. Analytical assessment of toppling

With the models PM-1 to PM-4 presented in Fig. 6, it is possible to develop simple 2D analytical predictions of the critical angle of toppling. To do that, some cross-sections were divided into simpler shapes (like squares, rectangles and triangles). The driving forces were located at the centroids of each subsection and the stabilizing and overturning moments were calculated by considering the rotation axis as the lower corner of the model in contact with the tilting table, which was also set as the origin of the coordinate system for calculations. The critical angle of toppling, α_{cr}, can easily be estimated by imposing a factor of safety, FS = 1 in Eq. 1.

Other scenarios, like those presented for models PM-5 to PM-7, require a more detailed analysis on the positioning of the *cog* as well as the rotation pivot.

It is relevant to note that the relative stability of any of the blocks under scrutiny for any position can be both computed in terms of factor of safety and in terms of critical stability angle. Obviously, these two approaches are related to one another, so they can be

computed for different scenarios. For test interpretation purposes where no additional actions exist (water pressures, earthquakes), the authors have selected the critical angle approach, thinking it could be more illustrative for output comparison purposes. However, a factor of safety approach could also be developed.

3.2.1. Symmetric model with straight edges and planar base

The simplest geometry studied (PM-1), consists of a symmetric block with a constant cross-section that can be divided in two triangles and a rectangle. The model is defined in terms of the central block breadth, *b*. A sketch of this model is presented in Fig. 10, where the relevant force components and the rotation axis for a given inclination of the base (α) are also shown.

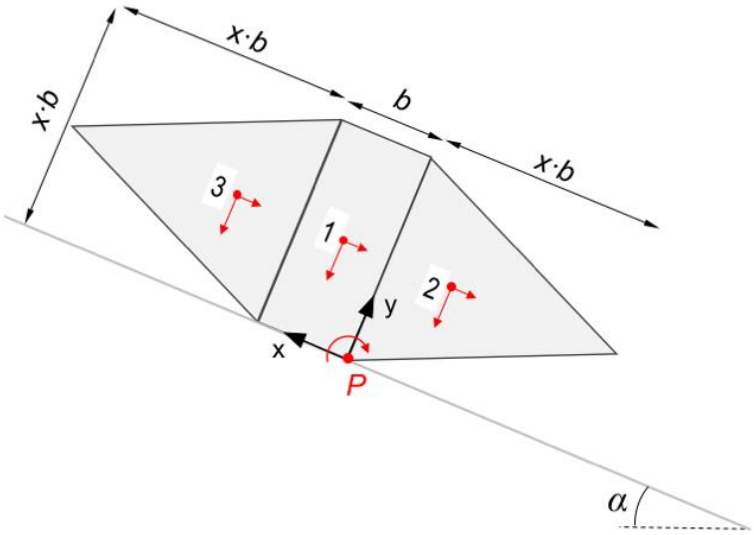

Fig. 10. Sketch of the symmetric model with constant cross-section, where the centroid of each sub-element is shown as well as the rotation pivot and origin of x-y coordinates.

For demonstrative purposes, we present the derivation of the critical angle formulation, based on the computation of the factor of safety for the rock block illustrated in Fig. 10. If one considers the rotation pivot (P) as the origin, the expression for estimating the factor of safety (*FS*) dividing the block in its three basic elements is as follows:

$$FS = \frac{\sum M_{stabilizing}}{\sum M_{overturning}} = \frac{W_1 \cos\alpha \, \frac{b}{2} - W_2 \cos\alpha \, \frac{xb}{3} + W_3 \cos\alpha \, \frac{(3+x)b}{3}}{W_1 \sin\alpha \, \frac{xb}{2} + W_2 \sin\alpha \, \frac{xb}{2} + W_3 \sin\alpha \, \frac{xb}{2}} \quad (5)$$

364

365 In this case, all forces acting parallel to the x-axis correspond strictly to destabilizing
366 moments, while those acting parallel to the y-axis contribute to both the stabilization (sub-
367 sections 1 and 3) and destabilization (sub-section 2) of the block shown in Fig. 10.

368

369 Accounting for the fact that $W_2 = W_3$, and that $W=W_1+W_2+W_3$, Eq. 5 can be simplified to
370 Eq. 6:

$$FS = \frac{\sum M_{stabilizing}}{\sum M_{overturning}} = \frac{W \cos\alpha \, \frac{b}{2}}{W \sin\alpha \frac{xb}{2}} = \frac{1}{x \cdot \tan\alpha} \quad (6)$$

371

372 Equating the *FS* to 1, the point at which instability initiates, the critical angle for toppling
373 in Fig. 10 can be derived as Eq. 7:

$$\alpha_{cr} = \operatorname{atan}\left(\frac{1}{x}\right) \quad (7)$$

374

375 This implies that, as mentioned above, the size of the sample does not influence results,
376 so the physical model represents the behavior of any smaller or larger homothetic block.
377 For the analyzed case and considering that $x = 2.7$, the critical angle in this case will be
378 $\alpha_{cr} = 20.32^{o}$ as derived from Eq. 7. The influence of the height of the central rectangular
379 block could be easily computed by testing different values of x in Eq. 7. This kind of
380 analytical solution is therefore quite suitable for evaluation of the influence of some
381 geometrical parameters of the blocks under scrutiny.

382

383 Alternatively, the *FS* can be computed for the case the *cog* is known from the beginning
384 accounting for the stabilizing and overturning moments of the weight as presented in Eq.
385 1. For blocks with more complex geometry, it therefore tends to be most convenient to
386 compute the position of the *cog* to simplify subsequent computations.

387

388

389

390

3.2.2. Asymmetric model with straight edges and planar base

This model (named as PM-2) presents an asymmetric cross-section that can be divided into simpler shapes (i.e. two rectangles and two triangles) to simplify calculations, as presented in Fig. 11.

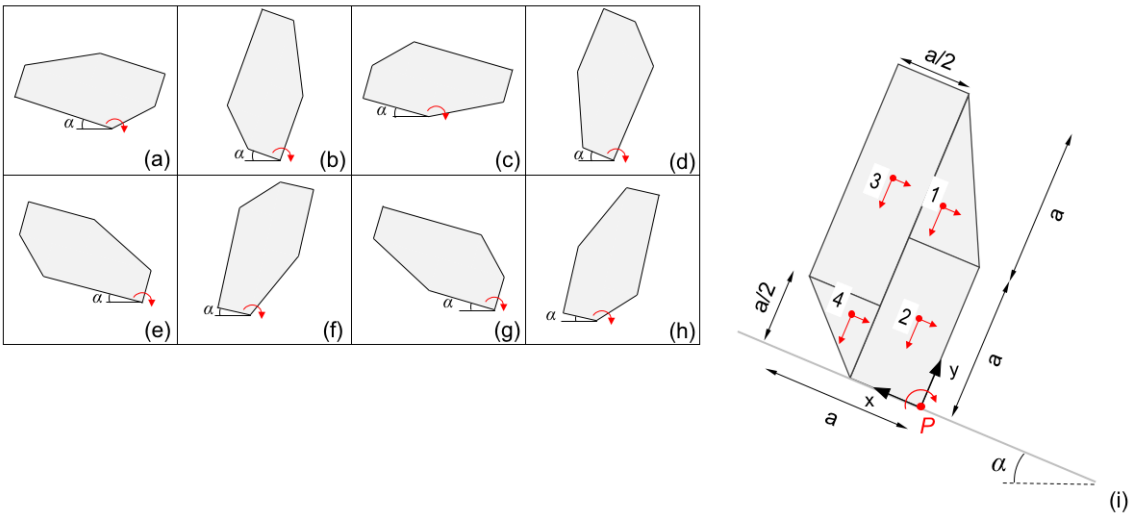

Fig. 11. Sketch of an asymmetric model with constant cross section and straight edges. All the possible testing positions for toppling analyses are presented (a-h). The sub-sections (1-4) indicated in the enlarged sketch (i) on the left are kept for all models.

For the model sketched in Fig. 11i (equivalent to that in Fig. 11b), the angle of critical toppling can be estimated with Eq. 8, in which the cross section was divided in four simpler subsections.

$$\alpha_{cr} = \arctan\left(\frac{W_1 \cdot \frac{a}{3} + W_2 \cdot \frac{a}{4} + W_3 \cdot \frac{3a}{4} + W_4 \cdot \frac{2a}{3}}{W_1 \cdot \frac{4a}{3} + W_2 \cdot \frac{a}{2} + W_3 \cdot \frac{5a}{4} + W_4 \cdot \frac{a}{3}}\right) \quad (8)$$

By modifying the position of the PM-2 block as presented in Fig. 11i, it is possible to get different geometries that will change the cross section to be analyzed, as shown in Fig. 11a-h and, consequently, the critical angle of toppling. This procedure is valuable when performing the experimental part of the present work, since it will allow testing a single model in eight different positions.

To illustrate how the stability against toppling and, ultimately, the critical angle of this relatively complex geometry block could be computed, the complete set of equations (Eq.

9-16) for calculating the analytical critical angle of toppling for each position of the block is presented in Table 1. Again, in this case, as in any other, the stability against toppling will be completely independent of the block size.

Table 1. Equations for estimating the FS against toppling and angles of critical toppling for all the positions presented in Fig. 10 (a-h).

Block position	Equation	
(a)	$\alpha_{cr} = \arctan\left(\frac{W_1 \cdot \frac{5a}{6} + W_3 \cdot \frac{3a}{4} - W_4 \cdot \frac{a}{6}}{W_1 \cdot \frac{2a}{3} + W_2 \cdot \frac{3a}{4} + W_3 \cdot \frac{a}{4} + W_4 \cdot \frac{a}{3}}\right)$	(9)
(b)	$\alpha_{cr} = \arctan\left(\frac{W_1 \cdot \frac{a}{3} + W_2 \cdot \frac{a}{4} + W_3 \cdot \frac{3a}{4} + W_4 \cdot \frac{2a}{3}}{W_1 \cdot \frac{4a}{3} + W_2 \cdot \frac{a}{2} + W_3 \cdot \frac{5a}{4} + W_4 \cdot \frac{a}{3}}\right)$	(10)
(c)	$\alpha_{cr} = \arctan\left(\frac{-W_1 \cdot \frac{a}{3} + W_2 \cdot \frac{a}{2} - W_3 \cdot \frac{a}{4} + W_4 \cdot \frac{2a}{3}}{W_1 \cdot \frac{a}{3} + W_2 \cdot \frac{a}{4} + W_3 \cdot \frac{3a}{4} + W_4 \cdot \frac{2a}{3}}\right)$	(11)
(d)	$\alpha_{cr} = \arctan\left(\frac{W_1 \cdot \frac{2a}{3} + W_2 \cdot \frac{3a}{4} + W_3 \cdot \frac{a}{4} + W_4 \cdot \frac{a}{3}}{W_1 \cdot \frac{2a}{3} + W_2 \cdot \frac{3a}{2} + W_3 \cdot \frac{3a}{4} + W_4 \cdot \frac{5a}{3}}\right)$	(12)
(e)	$\alpha_{cr} = \arctan\left(\frac{W_1 \cdot \frac{2a}{3} + W_2 \cdot \frac{3a}{2} + W_3 \cdot \frac{3a}{4} + W_4 \cdot \frac{5a}{3}}{W_1 \cdot \frac{2a}{3} + W_2 \cdot \frac{3a}{4} + W_3 \cdot \frac{a}{4} + W_4 \cdot \frac{a}{3}}\right)$	(13)
(f)	$\alpha_{cr} = \arctan\left(\frac{-W_1 \cdot \frac{a}{6} - W_2 \cdot \frac{a}{4} + W_3 \cdot \frac{a}{4} + W_4 \cdot \frac{a}{6}}{W_1 \cdot \frac{2a}{3} + W_2 \cdot \frac{3a}{2} + W_3 \cdot \frac{3a}{4} + W_4 \cdot \frac{5a}{3}}\right)$	(14)
(g)	$\alpha_{cr} = \arctan\left(\frac{W_1 \cdot \frac{4a}{3} + W_2 \cdot \frac{a}{2} + W_3 \cdot \frac{3a}{4} + W_4 \cdot \frac{a}{3}}{W_1 \cdot \frac{a}{3} + W_2 \cdot \frac{a}{4} + W_3 \cdot \frac{3a}{4} + W_4 \cdot \frac{2a}{3}}\right)$	(15)
(h)	$\alpha_{cr} = \arctan\left(\frac{W_1 \cdot \frac{a}{6} + W_2 \cdot \frac{a}{4} - W_3 \cdot \frac{a}{4} - W_4 \cdot \frac{a}{6}}{W_1 \cdot \frac{4a}{3} + W_2 \cdot \frac{a}{2} + W_3 \cdot \frac{5a}{4} + W_4 \cdot \frac{a}{3}}\right)$	(16)

3.2.3. Symmetric model with rounded edges and planar base

Another model presenting a symmetric cross-section is that corresponding to a rectangular prism with rounded corners (PM-3), as originally analyzed by Alejano et al. (2015). The cross-section of the model is shown in Fig. 12 and, due to the simplicity of this section, only the *cog* of the entire model was considered.

If the moment equilibrium calculation is performed for the model presented in Fig. 12, the angle of critical toppling can be estimated (Eq. 17) as rearranged from Eq. 4. Note that the addition of a non-zero radius of curvature (r) reduces the critical angle of toppling, since it decreases the actual contact width by $2r_c$.

$$\alpha_{cr} = \arctan\left(\frac{b - 2r_c}{h}\right) \tag{17}$$

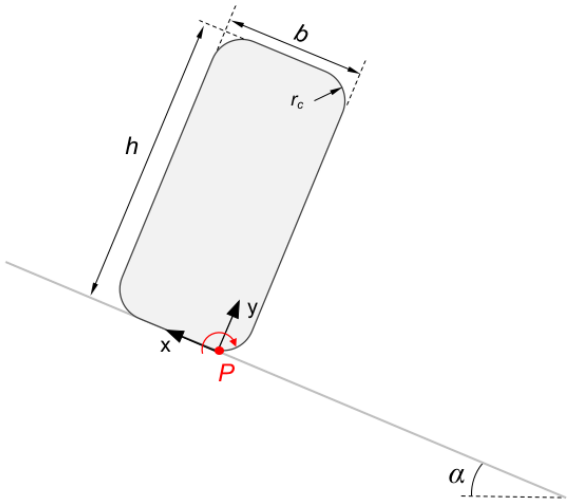

Fig. 12. Sketch of the symmetric model with rounded edges (for the studied model: h/b = 2.125 and r_c/h = 0.147).

3.2.4. Model with non-planar (concave) base

The present model is intended to illustrate the effect of a non-planar (concave) base, as a potentially stabilizing factor. The idea was to study a circular cross-section in which part of it is embedded in the inclined plane, resting on a concave base that coincides with the curvature of the cross section (see Fig. 7b and Fig. 13a).

It can be demonstrated that the angle of critical toppling, α_{cr}, of the model presented in Fig. 13a solely depends on the depth of the slot (s) relative to the radius of the circular cross-section (r), n, where $n = s/r$ for $n \in (0, 1)$. The angle of critical toppling can therefore be calculated from Eq. 18.

$$\alpha_{cr} = \operatorname{atan}\left\{\frac{\sin[\operatorname{acos}(1 - n)]}{1 - n}\right\} \tag{18}$$

With the aim of illustrating the effect of a concave contact on the angle of critical toppling of such a circular section of radius *r*, the critical angle is plotted against the depth of the slot expressed as a proportion of the radius (*n*) in Fig. 13b.

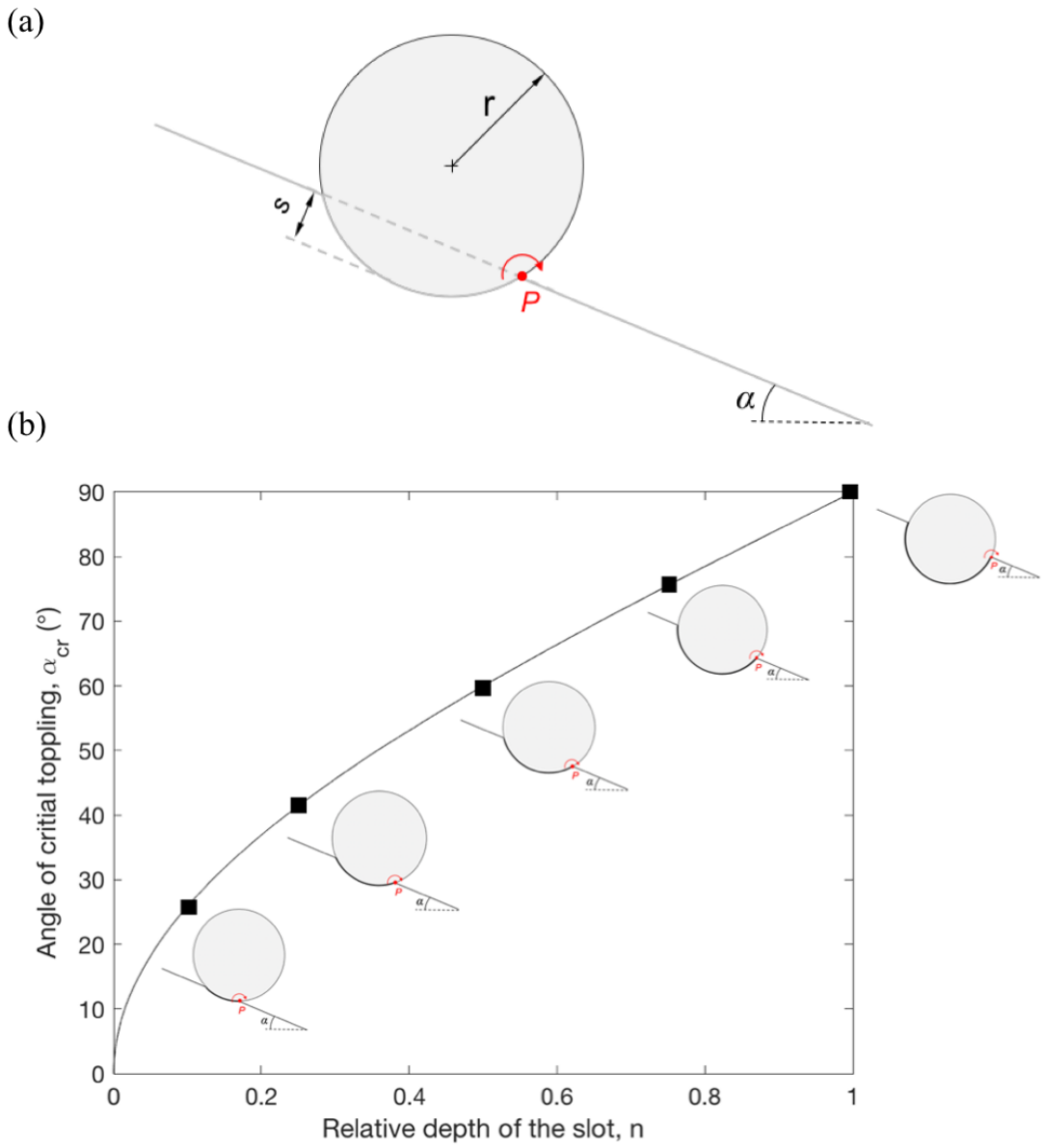

Fig. 13. (a) Sketch of the model with non-planar (concave) base; (b) Dependence of the angle of critical toppling (y-axis) with the relative depth of the slot, n (x-axis), for the model depicted in (a).

As is shown in Fig. 13b, the effect of a concave contact clearly influences the angle of critical toppling of a block with a circular section. This effect is most significant for low values of *n*, where the derivative $d\alpha_{cr}/dn$ is larger

Though almost no blocks are expected to match the geometry shown in Fig. 13a perfectly, in practice, these results mean that even relatively small concavities of the basal plane of

a block of more irregular shape have the potential to increase the angle of critical toppling by a few degrees.

3.2.5. Model with the *cog* not contained in a symmetry plane: squared/rectangular base

The position of the center of gravity (*cog*) clearly influences the toppling behavior of an element as in the case of the blocks already analyzed in this study. If a block is positioned onto a flat surface and the vertical projection of its *cog* falls inside the contact area, the block will remain stable against toppling. Consider the situation illustrated in Fig. 14a for a square-based, symmetric and homogeneous block. In this case, if the *cog* is projected onto the base, that projection will fall on the center of the square section. If the block is progressively tilted along the dash-dot plane, it will topple once the projection of the *cog* falls out the base.

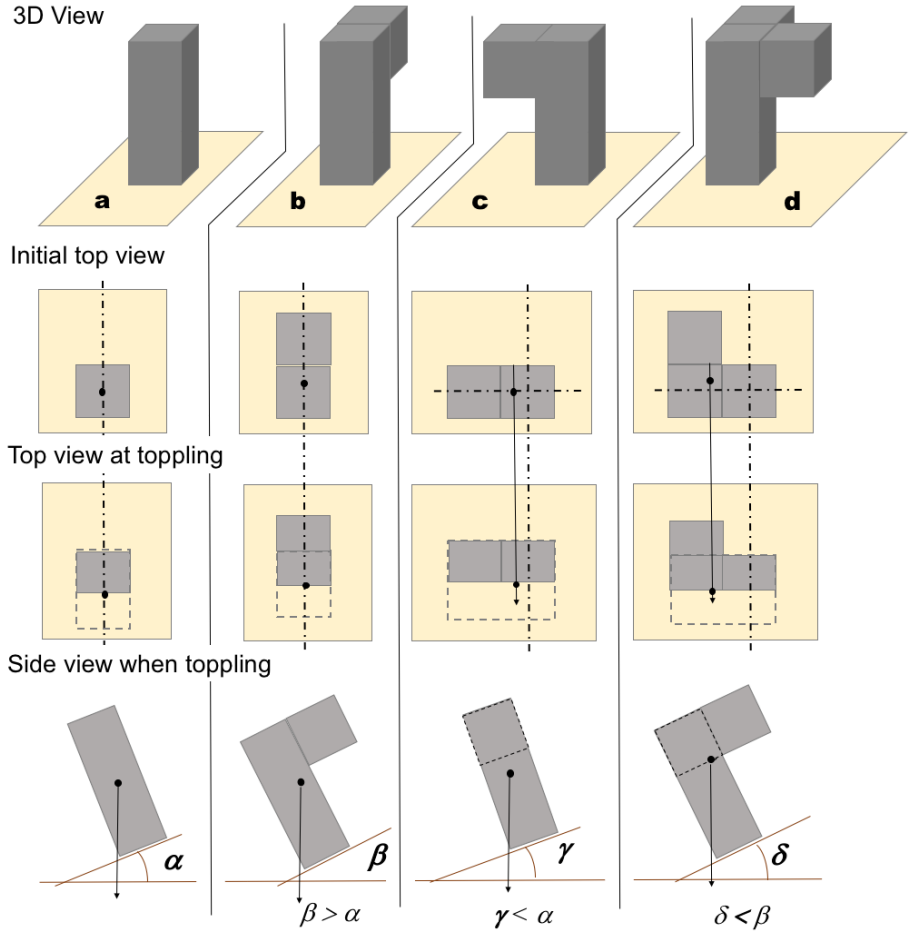

Fig. 14. Different 3D elements (a, b, c and d) to be subjected to a tilt test to illustrate the role of geometry on toppling. On the upper row, 3D view of the elements resting on a horizontal base to be tilted. On the second row, initial top view with the projection including the *cog*. On the third row, top view of the surface after tilting and in the moment of toppling and, on the last row, side view of platform and element when toppling.

Fig. 14b shows a more complex geometry with similar prism and cube attached to its upper back face. The *cog* of this model, when placed on a flat surface, will not project on the center of the base but will instead project somewhere behind the center of the base due to the added mass. Because of this, when tilting the plane where this element stands, it will topple at a higher angle than the previous case; in other words, the angle of critical toppling in this case (α) will be higher than the one observed for the element shown in Fig.14a (β).

The third element (Fig. 14c) is similar to element 'b', but the added cube is now attached on the upper part of a lateral face. Its *cog* will be at the same height as for element b (since it is the same element in the same position), but its projection onto a horizontal plane will be moved to the left in relation to element 'a' (Fig. 14c, second row). When tilting the platform where element 'c' rests, it will topple at a lower angle than α, because its *cog* is located higher than in case 'a', meaning its projection will fall outside its base at a lower angle γ, which will be also less steep than β.

Element 'd' is a rectangular prism with a square cross-section where two cubes are attached on the upper part of its lateral backward and leftward faces. In this case, the *cog* of the element will be even more displaced upwards than in the case of elements 'b' and 'c' and the *cog* projection on its base will be slightly moved backwards and a little bit to the left in relation to the case of element 'a' in Fig 14. This will clearly be less stable than 'b' (since the side-attached cubes displace the *cog* upwards) but more stable than 'c' (since the back-attached cube will increase its stability by moving the projection of its *cog* backwards). According to the previous analyses, a hierarchy on the angle of critical toppling can be stablished for the studied models shown in Fig. 14 as: $\beta > \delta > \alpha > \gamma$.

With the goal of assessing the effect of a displaced *cog* on the toppling behavior in a more detailed way and following the ideas described in the previous paragraphs, the model presented in Fig. 15 has been considered. It consists of a rectangular-based block with a small prismatic slab attached on the upper part of a lateral face (see Fig. 14b.1).

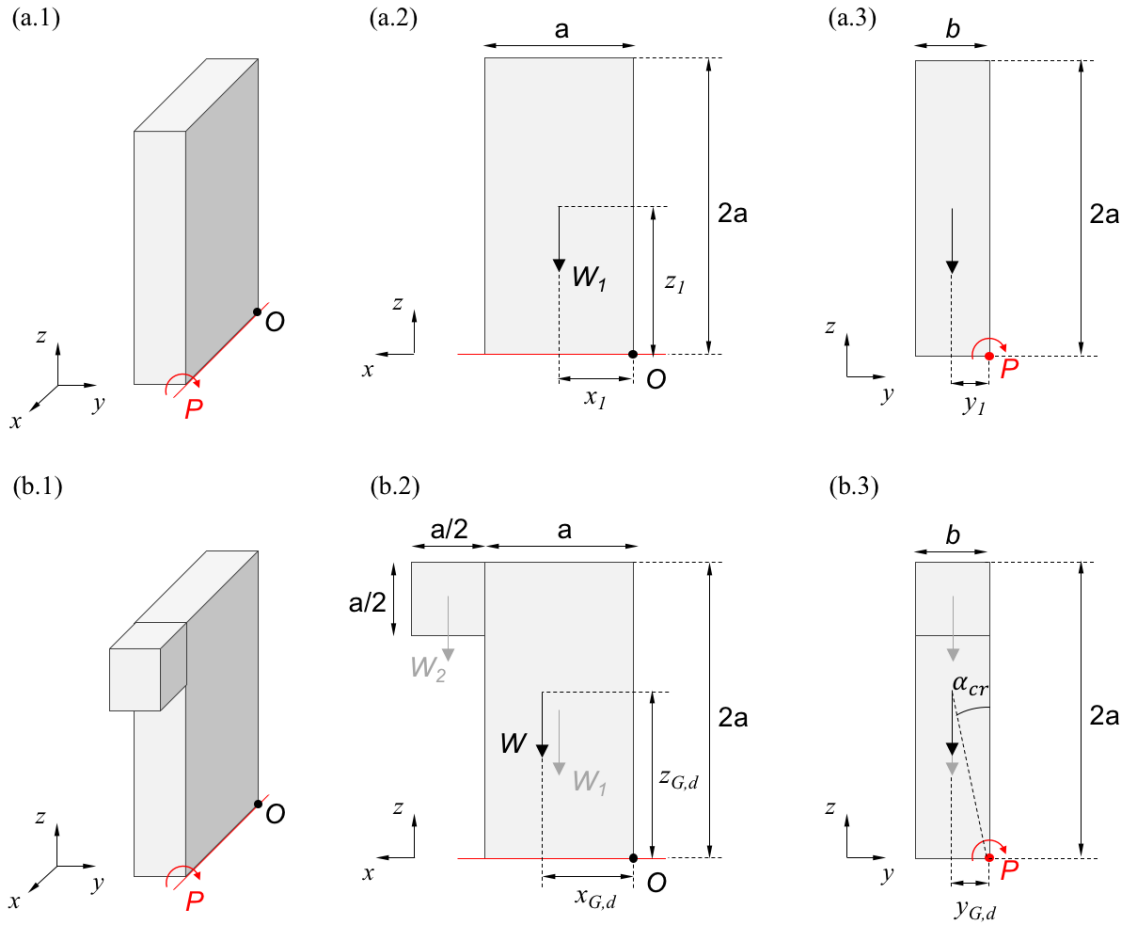

Fig. 15. (a) 3D view of the model with the axis of rotation and origin of coordinates for positioning the *cog* marked; (b) levelled front view of the assembly and (c) levelled lateral view of the assembly.

As previously mentioned, the effect of adding such a piece to a rectangular-based block as shown in Fig. 15 implies a displacement of the *cog*, which will move towards the added mass. This positioning of the *cog* can be easily determined by resorting to Eqs.19, 20 and 21 for each coordinate, respectively, when considering $m_i = W_i / g$.

$$x_{G,d} = \frac{\sum(m_i \cdot x_i)}{\sum m_i} \tag{19}$$

$$y_{G,d} = \frac{\sum(m_i \cdot y_i)}{\sum m_i} \tag{20}$$

$$z_{G,d} = \frac{\sum(m_i \cdot z_i)}{\sum m_i} \tag{21}$$

Once the 3D coordinates of the displaced *cog* are set ($x_{G,d}$, $y_{G,d}$, $z_{G,d}$), the angle of critical toppling for the model sketched in Fig. 15b.1 can be estimated using Eq. 22:

$$\alpha_{cr} = \text{atan}\left(\frac{y_{G,d}}{z_{G,d}}\right) \tag{22}$$

In a similar way as presented in Eq. 8, the angle of critical toppling can also be estimated as a function of dimensions *a* and *b* of the specimen (Eq. 23):

$$\alpha_{cr} = \text{atan}\left[\frac{(W_1 + W_2)\frac{b}{2}}{W_1 \cdot a + W_2 \cdot \frac{3a}{2}}\right] \tag{23}$$

It has to be highlighted that all the models with a rectangular or squared-base such as those shown in the previous sections and particularly the last shown in Fig. 15 will always have a pre-defined axis of rotation, which coincides with an edge of the block in contact with the base. This is not the case for circular or irregular-based specimens, as considered in Section 3.2.6.

3.2.6. Model with the *cog* not contained in a symmetry plane: circular base

Real rock blocks and boulders as found in Nature rarely have *cog*s that project in the center of their bases when resting on horizontal surfaces, nor do they have well-defined axes of rotation against toppling mechanism due to their typically irregular shapes. As already noted, for a precise assessment of their stability against toppling, it will be necessary to correctly position the *cog* as well as the pivot or axis around which the toppling mechanism will take place.

The study of these features has been carried out using a laboratory physical model (as shown in Fig. 6f) consisting of two cylinders composed of different materials (rock and steel with densities of ρ_r = 2700 kg/m^3 and ρ_s = 7900 kg/m^3, respectively). Both cylinders have the same radius (r = 27 mm) but different heights, with the rock cylinder measuring 100 mm in height and the steel cylinder measuring 35 mm in height. The assembly is sketched in Fig. 16b.1.

This test consisted of placing the two cylinders as shown in Fig. 16b.1, with the top piece displaced a distance of r/2 along the *x* direction. This position of the top steel cylinder moves the center of gravity out of the center of the base, as can be seen in the front view shown in Fig. 16c. Then, the specimen was progressively tilted (being the platform rotation around the x-axis) until toppling of the entire set occurred, when the tilting angle (angle of critical toppling) was reached.

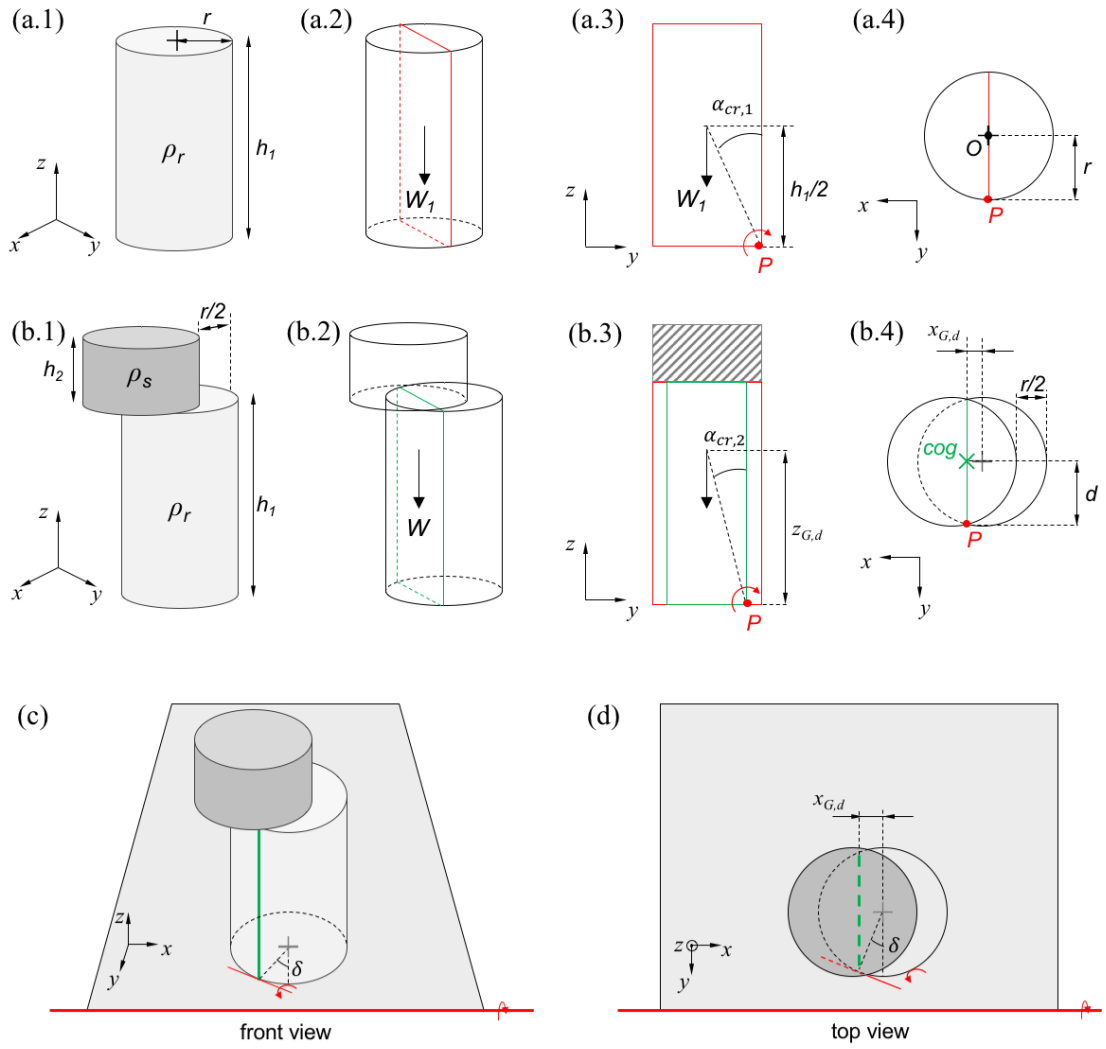

Fig. 16. (a.1-4), (b.1-4) Different views of the model containing the *cog* out of a symmetry axis (model PM-6); (c), (d) Different views of the model PM-6 at the equilibrium limit state, where the axis of rotation does not coincide with that of the rotating platform.

By considering the origin of the coordinate system at the center of the base of the lower cylinder (Fig. 16a.4), and regarding that $z_{g,d}$ can be easily obtained as function of the densities and block geometries, the angle of critical toppling for the model presented in Fig. 16b.1 when tilted around the x-axis can be calculated using Eq. 24.

$$\alpha_{cr} = \text{atan}\left(\frac{d}{z_{G,d}}\right) \quad (24)$$

Unlike the other examples considered in this study, this model will behave differently once the limit equilibrium for toppling has been reached. Specifically, although the critical angle of toppling can be calculated in a similar way to that of the other models (Eq. 12), the rotation of the cross-section containing the *cog* of the assembly (shown in green in Fig. 16b.3 and Fig. 16b.4) has to be considered, as it influences the rotation axis.

As shown in Fig. 16c, d, the axis (pivot) of rotation will not coincide with that of the rotating platform and will move laterally due to the displacement of the *cog* and the circular base in such a way that the new axis of rotation corresponds to the tangent at the intersection point between the plane containing the new *cog* (shown in green color in Fig. 16c, d) and the base of the model. The displacement angle, δ, as shown in Fig. 16d can be calculated using Eq. 25.

$$\delta = \text{asin}\left(\frac{x_{G,d}}{r}\right) \quad (25)$$

3.2.7. 3D-printed model representative of a real boulder

The last model (PM-7) considered in this study corresponds to a plastic (PLA) replica of a real granitic boulder located in the NW of Spain, as studied by Pérez-Rey et al. (2019). The replica, made at a scale of approximately 1:50, was created from an 3D point cloud of the real boulder collected in the field, which was afterwards processed with the software *CloudCompare* (Girardeau-Montaut, 2018) and *Meshlab* (Cignoni et al., 2008) in order to develop the 3D printing stage with a *BCN Sigma 3D* printer (see Fig. 17).

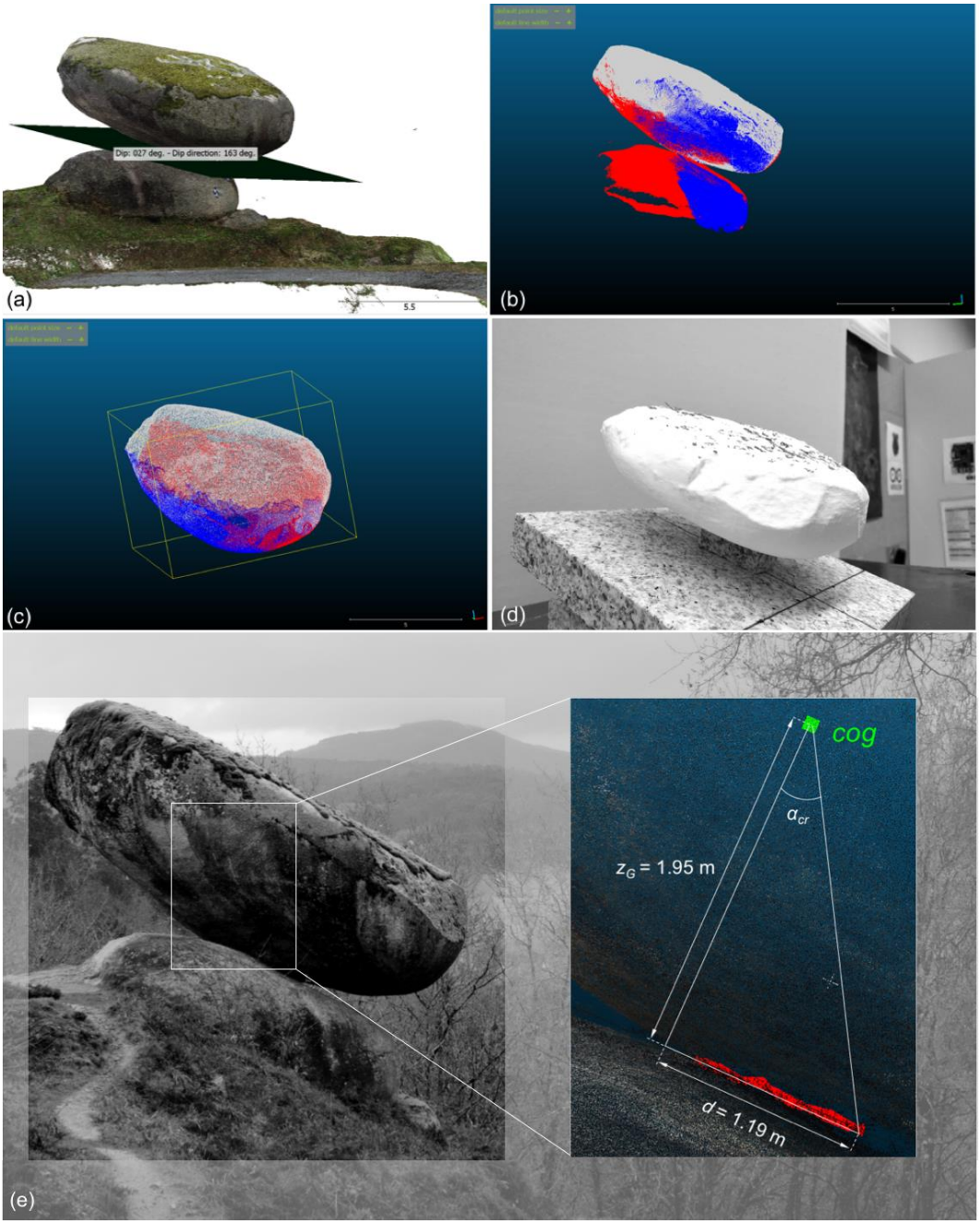

Fig. 17 (a, b) Two views of the 3D point cloud of the studied boulder; (c) Isolation of the boulder from the rest of the structure; (d) 3D-printed replica on the testing platform and (e) Detailed view of the position of the *cog* projected onto the contact plane, showing the distance *d* required for estimating the critical angle of toppling.

By taking advantage of such a precise 3D point cloud and with the assistance of *CloudCompare* software, it is possible to approximate, in a reasonable manner, the contact area between the boulder and the base and to position the *cog*.

Using the relationship presented in Eq. 23 and the geometrical parameters presented in Fig. 17e, it is possible to estimate the approximate angle of critical toppling of the boulder to be $\alpha_{cr} = 31.4°$.

4. Results

4.1. Comparison of analytical and experimental results

After carrying out all calculations of the angle of critical toppling of each of the models considered for this study, as presented in Section 3, all analytical results are shown in Table 1. Together with these results, the experimental angles of toppling obtained for each series of three tests carried out with the seven physical models are also provided with an averaged result. As it can observed in this table, the discrepancy of the analytical and average laboratory results is always less than 1.3º, and the median error is 0.66º.

It must be noted that some models did not achieve toppling failure in the laboratory tests (in particular, the PM-2 model in some positions). This occurs when the theoretical toppling angle is greater than the basic friction angle of the base contact surface, and the block slides before reaching its toppling angle. These results are indicated in Table 2 with an 's'. It has also been observed that PM-2 model in position (h) was not self-stable in a horizontal position ($\alpha_{cr} < 0$).

Table 2. Analytical and experimental results for the angle of critical toppling (in degrees) as obtained for the seven studied models.

Model	Position	Analytical	Experimental (s = slide)			
		α_{cr}	α_1	α_2	α_3	α_{mean}
PM-1	—	20.32	20.2	20.3	20.5	20.3
PM-2	(a)	44.22	30.4 (s)	27.2 (s)	30.1 (s)	29.2 (s)
	(b)	28.66	29.1	29.0	29.2	29.1
	(c)	4.18	3.2	3.2	3.1	3.2
	(d)	24.55	25.4	25.3	25.6	25.4
	(e)	65.45	33.5 (s)	30.9 (s)	27.0 (s)	30.5 (s)
	(f)	1.41	2.6	2.7	2.7	2.7
	(g)	61.34	29.0 (s)	25.6 (s)	26.5 (s)	27.0 (s)
	(h)	< 0	—	—	—	—
PM-3	—	10.01	11.0	11.0	9.67	10.6
PM-4	(a) (n =1/6)	33.56	33.3	32.5	32.8	32.9
	(b) (n=1/3)	48.19	47.3	48.3	48.4	48.0
PM-5	—	11.88	11.6	12.3	12.4	12.1
PM-6	—	17.29	16.5	15.9	16.2	16.2
PM-7	—	31.39	30.8	30.4	30.7	30.6

4.2. 3D discrete numerical modelling

Another way to validate the results of the physical models is by comparing these results with those obtained by numerical analysis. For this part of the study, we have utilized the Distinct Element Method (DEM), which applies an explicit finite difference method for modelling large displacements and rotations of block systems (Cundall, 1971). This method has been used in numerous studies of toppling (Brideau and Stead, 2010; Lanaro et al., 1997; Pritchard and Savigny, 1990). In this case, we used the DEM as implemented in the software 3DEC v5.20 (Itasca, 2016).

Discrete Element Methods can deal with geological structures of any size and shape, and with a great variety of constitutive models for both the intact rock and the discontinuities. They also allow for simulation of complex hydrogeological environments or time-dependant phenomena like rock-dynamics or creep. Another advantage of this study is that it does not require the prior definition of a displacement direction (as required in the analytical calculation), meaning the results of the other methods can be confirmed in cases where there is any doubt about the displacement direction, such as for models with a displaced *cog* (PM-5 and PM-6), or the model with the irregular, complex shape (PM-7). The same tilt tests performed with the physical models were simulated in 3DEC (Fig. 18).

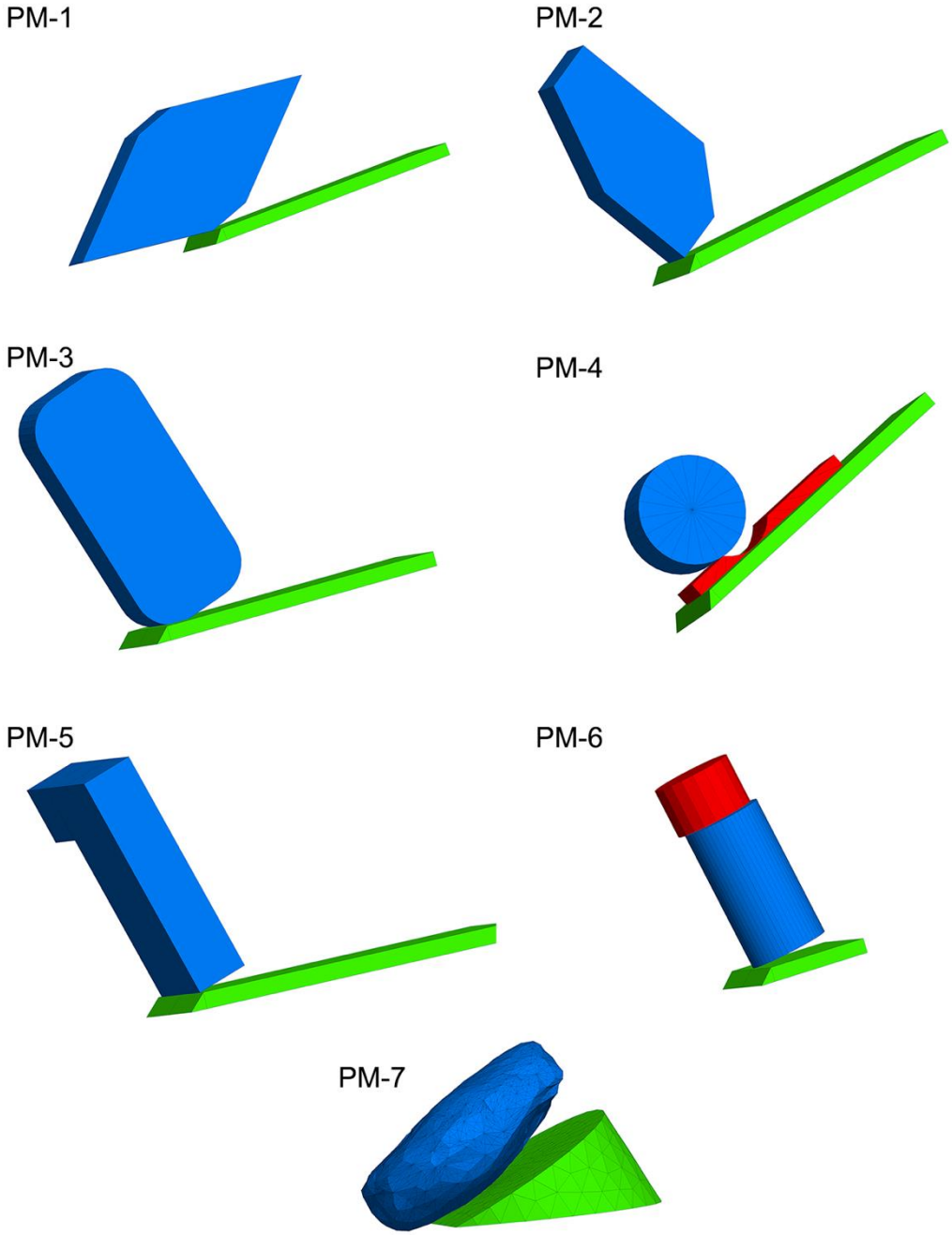

Fig. 18. Results for the numerical simulation of the tilt tests performed.

In these models, both the tilt table and the specimens were modelled as rigid blocks. The contact stiffnesses were set to k_n 650 GPa/m and k_s 150 GPa/m. The tilting rate was set slow enough to ensure that no inertial effect was produced so the test could be considered quasi-static. The results of these models are presented in Table 3, where the maximum difference observed between results obtained using various methods is displayed.

Table 3. Angles of critical toppling calculated by different methods and absolute maximum difference between results. Involved methods indicated in brackets.

Model	Angle of critical toppling (º)			Absolute max. difference (º)
	Experimental (E)	Analytical (A)	DEM (D)	
PM-1	20.3	20.32	20.1	0.22 (E-A)
PM-2	29.1	28.66	28.6	0.5 (E-N)
PM-3	10.6	10.01	10.0	0.6 (E-N)
PM-4	48.0	48.19	48.1	0.19 (E-A)
PM-5	12.1	11.88	11.9	0.22 (E-A)
PM-6	16.2	17.29	17.3	1.1 (E-N)
PM-7	30.6	31.39	31.3	0.79 (E-A)

The results obtained using the DEM models agree with those obtained by both the physical models and the analytical method, even in the cases where the centre of gravity is not located in the plane of symmetry, or the toppling involves complex movement not parallel to the tilting direction, as in the case of PM-6 (Fig. 19a).

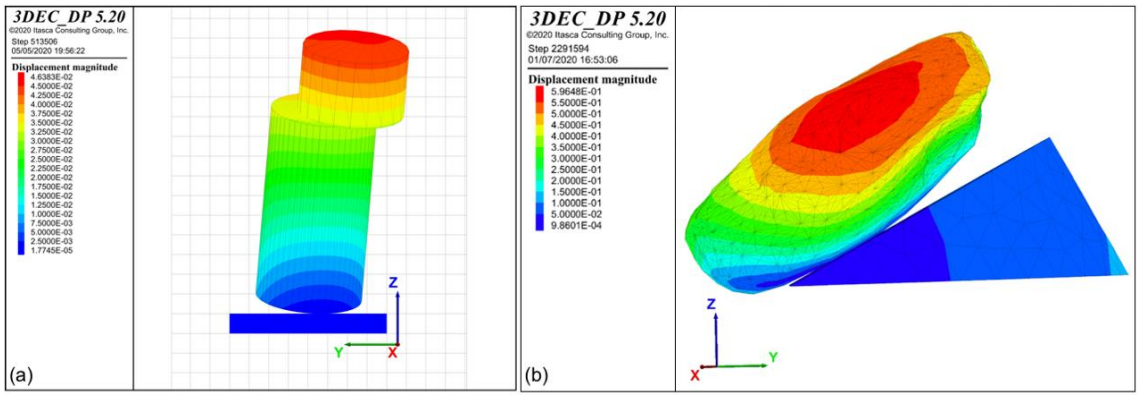

Fig. 19. (a) 3DEC results of the tilt simulation on a rock + steel set with and upper cylinder uncentered r/2 to the left (PM-6). After the block starts to topple, its movement does not follow the tilting direction because the *cog* is not located in the symmetry plane as assumed in section 3.2.6. (b) Displacement magnitude after tilt-test of PM-7 calculated by 3DEC.

It is relevant to note that the DEM and the analytical approach match so closely here (and in fact in general). This suggests that the errors observed in the experimental results are largely a function of limitations in the "manufacturing" processes used to build the various physical models.

The critical angle in models with complex geometries (PM-7) measured by the three methods were also similar, confirming the validity of both the experimental and the analytical approaches. This model (Fig. 19b) presents both an asymmetrical geometry and an irregular base shape, resulting in complex movement after destabilization.

5. Discussion

It is not difficult to find in Nature rock blocks or groups of blocks that could potentially become unstable due to toppling. In some case, these blocks are irregular enough so as to be considered heritage or part of natural parks, so they are preserved (Fig. 20). On the other hand, the instability of some other less aesthetically appealing rock blocks may jeopardize infrastructure or even people, lives and properties. In any of these cases, it is important to be able to analyze the stability of these blocks under different conditions such that appropriate protective measures can be defined.

Fig. 20. Balanced stones in Natural Parks. (a) 'The Three Sisters' balancing rocks, Matopos National Park, Matabeleland, Zimbabwe (b) *Roque de García*, basaltic horn at Teide National Park, Tenerife, Canary Islands, Spain (c) 3,500 t balanced rock, Arches National Park, Utah, USA and (d) 700 t balanced rock, 'The Garden of Gods', Colorado Springs, USA. Photos by the authors.

Although some approaches were developed in the past to compute the stability of blocks against toppling, in many cases, and specifically those corresponding to complex geometry blocks, it was indeed difficult to accurately compute stability against toppling. Recent advances in theoretical stability analysis based on idealized geometries (rounded corners, concave or convex surfaces) have contributed to a better understanding of toppling phenomena. The approaches presented here based on modern block geometry reconstruction methods, 3D printing of a block replica and testing of this replica using a tilt table, help to reproduce the potential instability phenomena of these blocks and to assess their 'degree of stability' or instability, i.e., how far from toppling they are.

One notable limitation of the approach demonstrated in this study is the lack of knowledge of the geometry (concavity or concaveness and roughness) of the contact between the block and the surface where it rests, as well as its actual frictional behavior. However, the proposed approach, in combination with detailed in-situ characterization and the application of analytical and numerical calculation techniques as illustrated in this document, has the potential to contribute to improved assessments of the stability of irregular rock blocks or boulders.

6. Concluding remarks

All over the world, and particularly in mountainous terrain in hot and temperate regions, rock blocks or boulders occur, and may exist in a state of marginal stability. In most of these cases, the potential instability of these blocks does not represent a hazard to human life or property. In some cases, however, it may be important to quantify block stability either due to an associated hazard, or due to its significance to the community or its natural landscape value.

Analyzing the stability of these blocks is not an easy task, primarily due to their complex geometry and because it is also difficult to characterize in sufficient detail all the features actually affecting their stability, including block geometry, geometry of the contact with the base surface, strength and deformability characteristics of this contact —of particular relevance when considering rough joints and infill material with non-negligible tensile strength—, and potential triggers such as water pressure or earthquake loading.

Recently developed remote-sensing tools, such as photogrammetry or LiDAR can be used in order to recover a rather accurate geometry of a block of interest as well as an approximate representation of the contact area (typically hidden). Based on the recovered 3D point cloud, a scaled physical model of the rock block or boulder can be 3D-printed, and its toppling behavior physically analyzed using a tilting platform, since toppling is exclusively dependent on the geometry of the potentially overturning object and the concavity of the base. This approach can be applied in combination with analytical or numerical techniques to study the mechanisms involved and to check physical testing results.

Acknowledgements

The last author acknowledges the Spanish Ministry of Universities for funding of his work in the project, awarded under Contract Reference No. RTI2018-093563-B-I00, partially financed by means of ERDF funds from the EU.

References

Akbarpour, T., Amini, M., Zamani, Z., 2012. Stability Analysis of Block Toppling Failures in Tunnels Portals of “Moshampa" Dam in Iran, in: Mechanics, K.S. for R. (Ed.), ISRM Regional Symposium - 7th Asian Rock Mechanics Symposium, 15-19 October, Seoul, Korea.

Al Mandalawi, M., You, G., Dahlhaus, P., Dowling, K., Sabry, M., 2019. Analysis of a Combined Circular--Toppling Slope Failure in an Open--Pit, in: Wasowski, J., Dijkstra, T. (Eds.), Recent Research on Engineering Geology and Geological Engineering. Springer International Publishing, Cham, pp. 10–30.

Alejano, L.R., Carranza-Torres, C., Giani, G., Arzúa, J., 2015. Study of the stability against toppling of rock blocks with rounded edges based on analytical and experimental approaches. Eng. Geol. 195, 172–184. https://doi.org/10.1016/j.enggeo.2015.05.030

Alejano, L.R., Castro-Filgueira, U., Pérez-Rey, I., Arzúa, J., 2017. Stability Analysis of an Over-tilted Slope in a Granite Quarry: The Role of Joint Spacing, in: Procedia Engineering. https://doi.org/10.1016/j.proeng.2017.05.197

Alejano, L.R., Ferrero, A.M., Ramírez-Oyanguren, P., Álvarez Fernández, M.I., 2011.

752 Comparison of limit-equilibrium, numerical and physical models of wall slope
753 stability. Int. J. Rock Mech. Min. Sci. 48, 16–26.
754 https://doi.org/https://doi.org/10.1016/j.ijrmms.2010.06.013

755 Alejano, L.R., García-Cortés, S., García-Bastante, F., Martínez-Alegría, R., 2013. Study
756 of a rockfall in a limy conglomerate canyon (Covarrubias, Burgos, N. Spain).
757 Environ. Earth Sci. 70, 2703–2717. https://doi.org/10.1007/s12665-013-2327-x

758 Alejano, L.R., Gómez-Márquez, I., Martínez-Alegría, R., 2010a. Analysis of a complex
759 toppling-circular slope failure. Eng. Geol. 114, 93–104.
760 https://doi.org/10.1016/J.ENGGEO.2010.03.005

761 Alejano, L.R., Ordóñez, C., Armesto, J., Rivas, T., 2010b. Assessment of the instability
762 hazard of a granite boulder. Nat. Hazards 53, 77–95.
763 https://doi.org/10.1007/s11069-009-9413-0

764 Alejano, L.R., Veiga, M., Gómez-Márquez, I., Taboada, J., 2012. Stability of granite
765 drystone masonry retaining walls: II. Relevant parameters and analytical and
766 numerical studies of real walls. Géotechnique 62, 1027–1040.
767 https://doi.org/10.1680/geot.10.P.113

768 Amini, M., Ardestani, A., 2019. Stability analysis of the north-eastern slope of Daralou
769 copper open pit mine against a secondary toppling failure. Eng. Geol. 249, 89–101.
770 https://doi.org/https://doi.org/10.1016/j.enggeo.2018.12.022

771 Armesto, J., Ordóñez, C., Alejano, L.R., Arias, P., 2009. Terrestrial laser scanning used
772 to determine the geometry of a granite boulder for stability analysis purposes.
773 Geomorphology 106, 271–277.
774 https://doi.org/https://doi.org/10.1016/j.geomorph.2008.11.005

775 Ashby, J.P., 1971. Sliding and toppling modes of failure in models and jointed rock
776 slopes (MSc thesis). London University - Imperial College (London).

777 Bader, C., Kolb, D., Weaver, J.C., Sharma, S., Hosny, A., Costa, J., Oxman, N., 2018.
778 Making data matter: Voxel printing for the digital fabrication of data across scales
779 and domains. Sci. Adv. 4, eaas8652. https://doi.org/10.1126/sciadv.aas8652

780 Barton, N., 1971. A model study of the behaviour of steep excavated rock slopes.
781 University of London (Imperial College of Science and Technology).

Bray, J.W., 1969. Seminar on toppling failure. London.

Bray, J.W., Goodman, R.E., 1981. The theory of base friction models. Int. J. Rock Mech. Min. Sci. Geomech. Abstr. 18, 453–468. https://doi.org/https://doi.org/10.1016/0148-9062(81)90510-6

Brideau, M.-A., Stead, D., 2010. Controls on Block Toppling Using a Three-Dimensional Distinct Element Approach. Rock Mech. Rock Eng. 43, 241–260. https://doi.org/10.1007/s00603-009-0052-2

Cai, J., Ju, N., Huang, R., Zheng, D., Zhao, W., Li, L., Huang, J., 2019. Mechanism of toppling and deformation in hard rock slope: a case of bank slope of Hydropower Station, Qinghai Province, China. J. Mt. Sci. 16, 924–934. https://doi.org/10.1007/s11629-018-5096-x

Christianson, M., Itoh, J., Nakaya, S., 1995. Seismic analysis of the 25 Stone Buddhas Group at Hakone, Japan. 35th U.S. Symp. Rock Mech.

Cignoni, P., Callieri, M., Corsini, M., Dellepiane, M., Ganovelli, F., Ranzuglia, G., 2008. MeshLab: an Open-Source Mesh Processing Tool, in: Scarano, V., Chiara, R. De, Erra, U. (Eds.), Eurographics Italian Chapter Conference. The Eurographics Association. https://doi.org/10.2312/LocalChapterEvents/ItalChap/ItalianChapConf2008/129-136

Cundall, P.A., 1971. A computer model for simulating progressive, large scale movements in blocky rock systems., in: Proceedings of the International Symposium on Rock Fracture, Vol.1. ISRM, Nancy, France, p. Paper II-8.

Domokos, G., Sipos, A.Á., Szabó, T., 2012. The Mechanics of Rocking Stones: Equilibria on Separated Scales. Math. Geosci. 44, 71–89. https://doi.org/10.1007/s11004-011-9378-x

Ferrero, A., Migliazza, M., Roncella, R., Segalini, A., 2011. Rock cliffs hazard analysis based on remote geostructural surveys: The Campione del Garda case study (Lake Garda, Northern Italy). Geomorphology 125, 457–471. https://doi.org/https://doi.org/10.1016/j.geomorph.2010.10.009

Ferrero, A.M., Forlani, G., Roncella, R., Voyat, H.I., 2009. Advanced Geostructural

812 Survey Methods Applied to Rock Mass Characterization. Rock Mech. Rock Eng.
813 42, 631–665. https://doi.org/10.1007/s00603-008-0010-4

814 Girardeau-Montaut, D., 2018. CloudCompare.

815 Goodman, R., Bray, J., 1976. Toppling of rock slopes, in: Proceedings of the Specialty
816 Conference on Rock Engineering for Foundations and Slopes. Vol. 2.

817 Guo, S., Qi, S., Yang, G., Zhang, S., Saroglou, C., Guo, S., Qi, S., Yang, G., Zhang, S.,
818 Saroglou, C., 2017. An Analytical Solution for Block Toppling Failure of Rock
819 Slopes during an Earthquake. Appl. Sci. 7, 1008.
820 https://doi.org/10.3390/app7101008

821 Hencher, S.R., 2015. Practical Rock Mechanics. CRC Press (Taylor and Francis
822 Group), Boca Raton, FL.

823 Hoek, E., Bray, J., 1974. Rock Slope Engineering. Chapman & Hall.

824 Itasca, 2016. 3 Dimensional Distinct Element Code. 3DEC.

825 Lanaro, F., Jing, L., Stephansson, O., Barla, G., 1997. DEM modelling of laboratory
826 tests of block toppling. Int. J. rock Mech. Min. Sci. Geomech. Abstr. 34, 506–507.
827 https://doi.org/10.1016/s1365-1609(97)00116-0

828 Müller, L., 1968. New considerations of the Vaiont slide. Felsmechanik und
829 engenieurgeologie 6, 1–91.

830 Pérez-Rey, I., Alejano, L.R., Riquelme, A., González-deSantos, L., 2019. Failure
831 mechanisms and stability analyses of granitic boulders focusing a case study in
832 Galicia (Spain). Int. J. Rock Mech. Min. Sci. 119, 58–71.
833 https://doi.org/https://doi.org/10.1016/j.ijrmms.2019.04.009

834 Pritchard, M.A., Savigny, K.W., 1990. Numerical modelling of toppling. Can. Geotech.
835 J. 27, 823–834. https://doi.org/10.1139/t90-095

836 Riquelme, A., Abellán, A., Tomás, R., Jaboyedoff, M., 2014. A new approach for semi-
837 automatic rock mass joints recognition from 3D point clouds. Comput. Geosci. 68,
838 38–52. https://doi.org/https://doi.org/10.1016/j.cageo.2014.03.014

839 Sagaseta, C., 1986. On the modes of instability of a rigid block on an inclined plane.
840 Rock Mech. Rock Eng. 19, 261–266. https://doi.org/10.1007/BF01039998

Shi, B., Anooshehpoor, A., Zeng, Y., Brune, J.N., 1996. Rocking and overturning of precariously balanced rocks by earthquakes. Bull. Seismol. Soc. Am. 86, 1364–1371.

St. John, C.M., 1972. Numerical and observational methods of determining the behaviour of rock slopes in opencast mines. University of London - Imperial College of Science and Technology.

Terzaghi, K., 1962. Stability of steep slopes on hard unweathered rock. Géotechnique 12, 251–270.

Tu, X., Dai, F., Lu, X., Zhong, H., 2007. Toppling and stabilization of the intake slope for the Fengtan Hydropower Station enlargement project, Mid-South China. Eng. Geol. 91, 152–167. https://doi.org/https://doi.org/10.1016/j.enggeo.2007.01.009

Vann, J.D., Olaiz, A.H., Morgan, S., Zapata, C., 2019. A Practical Approach to a Reliability-Based Stability Evaluation of Precariously Balanced Granite Boulders, in: Proceedings of the 53rd U.S. Rock Mechanics/Geomechanics Symposium. ARMA, New York, USA.

Virtanen, J.P., Hyyppä, H., Kurkela, M., Vaaja, M., Alho, P., Hyyppä, J., 2014. Rapid Prototyping — A Tool for Presenting 3-Dimensional Digital Models Produced by Terrestrial Laser Scanning. Int. J. Geo-Information 3, 871–890.

Yeung, M.R., Wong, K.L., 2007. Three-dimensional Kinematic Conditions For Toppling, in: 1st Canada - U.S. Rock Mechanics Symposium. American Rock Mechanics Association, Vancouver, Canada, p. 5.

Zábranová, E., Matyska, C., Stemberk, J., Málek, J., 2020. Eigenoscillations and Stability of Rocking Stones: The Case Study of “The Hus Pulpit” in The Central Bohemian Pluton. Pure Appl. Geophys. 177, 1907–1916. https://doi.org/10.1007/s00024-019-02296-z

Laboratory physical modelling of block toppling instability by means of tilt tests

HIGHLIGHTS

- Physical modelling represents an effective method for toppling-stability assessment
- Tilt-testing of small scale rock elements reproduce mechanisms at larger scales
- Different parameters influencing toppling behaviour have been analysed
- 3D point clouds of rock structures can be obtained from TLR and UAV photos
- 3D Distinct Element methods allow stability calculations of odd-shaped rocks

Laboratory physical modelling of block toppling instability by means of tilt tests

Ignacio Pérez-Rey[a,*], Mauro Muñiz-Menéndez[a], Javier González[b], Federico Vagnon[c], Gabriel Walton[d], Leandro R. Alejano[e,d]

[a]*Laboratorio de Geotecnia, CEDEX, Madrid, Spain*

[b]*Departamento de Ingeniería Metalúrgica y Minas, Universidad Católica del Norte, Antofagasta, Chile*

[c]*Department of Earth Science, Università degli Studi di Torino, Torino, Italy*

[d]*Department of Geology and Engineering Geology, Colorado School of Mines, Golden, USA*

[e]*Department of Natural Resources and Environmental Engineering, University of Vigo, Vigo, Spain*

[*]*corresponding author: ignacio.perez@cedex.es*

ABSTRACT

In this paper we introduce a physical modelling approach where the stability of rock blocks against toppling in the field can be estimated using a tilt table, engineered rock models and 3D-printed small-scale versions of a natural rock boulder. To achieve this goal, first, simple geometry rock elements are tilted and results interpreted according to analytical formulations. Then, more complex geometry engineered rock blocks, including some where its center of gravity does not project on the center of the base element, are tested and results properly interpreted. Eventually, the 3D-printed version of the rock boulder is produced from 3D point clouds recovered in the field by means of a combination of photogrammetry and laser scanner techniques. Analytical formulations and numerical calculations have been used in order to validate the proposed approach, to explain the physical phenomena involved, and to allow for possible extension of the physical modelling observations to different scenarios, such as those considering the influence of water or seismic loading on stability.

List of symbols

α	base plane inclination angle
α_{cr}	critical angle of toppling
b	width of the block
cog	center of gravity
ϕ	friction angle
FS	factor of safety
g	acceleration of gravity (9.81 m/s^2)
h	height of the block or model
P	rotation pivot of a given block or model and origin of the (x_i, y_i) coordinates
r	radius
r_c	roundness of the block corners (expressed as the radius of curvature)
x_i	distance from P to the cog of the i-th sub-section along the x-axis for a given block or model
y_i	distance from P to the cog of the i-th sub-section along the y-axis for a given block or model
w	width of the block (out of plane)
W	weight
W_i	weight of the i-th section

1. Introduction

Analysing the stability of natural or man-made slopes in rock masses is a complex task. The principles of the discipline addressing this problem (typically known as rock slope engineering) were established in the seminal works developed during the 1960s and 1970s at Imperial College in London and by Richard Goodman in Berkeley and summarized in the book entitled "Rock Slope Engineering" (Hoek and Bray, 1974; Wyllie and Mah, 2004). In this book, it was clearly stated that, unlike in the case of soils, where all the failure mechanisms involve sliding along a rotational or planar sliding surface, for rocks, a variety of failure mechanisms could occur according to the number, continuity, spacing, orientation and geomechanical characteristics of existing discontinuity sets.

Four typical types of failure mechanisms were identified at the time as the most common possibilities in rock slopes: planar, wedge, (block) toppling and circular failure. This classification combined with the simple mathematical tools provided to analyse their stability, represented a significant step forward in the rock engineering field, leading to improved rock slope stability analyses and designs. However, as wisely noted in the preface of Hoek and Bray's (1974) book, 'Because the rock mass behind every slope is unique, there are no standard recipes or routine solutions which are guaranteed to produce the right answer each time they are applied'. This is why it is important to bear in mind that rock slope instability phenomena do not necessarily occur according to simple failure mechanisms as those described in these early works.

Whereas three of these basic mechanisms refer to sliding phenomena, only one of them involves toppling. Toppling corresponds to rotation of relatively slender rock columns or blocks about a fixed base. There are two distinct types of toppling failure mechanisms named block and flexural toppling (Goodman and Bray, 1976). In the first case, the toppling block is already fully detached from the rest of the rock mass. The second implies flexural or tensile failure, where the block is not completely detached of the rock mass such that new tensile failure cracks need to occur to fully detach the block from the surrounding ones for toppling instability to occur. In this study we focus on the analysis of block toppling.

The simplest toppling case as considered by this study is that of a single toppling block. The first analyses of the stability against toppling of a single block were performed by Ashby (1971) and then extended and formalized by other authors (Hoek and Bray, 1974; Sagaseta, 1986). All these analyses start with stringent geometrical assumptions considering perfectly rectangular blocks with sharp corners resting on a tilted plane striking in the same direction as the block face in contact with the plane.

Some studies have recently begun to address the influence of more realistic shapes of blocks on block stability against toppling. Alejano et al. (2015) studied the influence of the rounding of block corners on the stability of a block. This geometric condition observed in some rock masses and associated with spheroidal weathering erosive processes was shown to significantly affect stability of blocks. The authors proposed a formulation to compute the stability of a round-cornered block to account for this effect. This formulation relies on the position of the potential rotation axis and was verified using physical models and field observations. While such a contribution is interesting and extends the type of toppling instability that can be analyzed, when one visits certain natural rock environments, it can be observed that many more complex irregular block geometries exist for which no analysis methods exist.

As an example, Fig. 1 illustrates three zones in two different mountain environments, where a number of toppled and stable blocks are observed. In most of the cases and based on our current capabilities to analyze stability of blocks, it would be indeed difficult to rigorously perform a back analysis of the instability or stability of these blocks to explain why are they stable or unstable. For the stable blocks, it would also be difficult to assess their stability after a potential change in loading conditions, such as in the case of a seismic event. Accordingly, the main goal of this study is to develop a methodology through which the stability of complex blocks (such as those illustrated in Fig. 1) can be rigorously analyzed.

Since the early studies, the authors have considered cases involving increasingly complex estimates of the toppling stability of individual rock blocks taking into account the occurrence of rounded corners on the toppling blocks (Alejano et al., 2017) or rock boulders (Alejano et al., 2010b; Pérez-Rey et al., 2019) and considered other studies available from literature focusing on the potential destabilizing effects of earthquakes on

rock blocks or groups of rock blocks (Christianson et al., 1995; Shi et al., 1996; Vann et al., 2019) where it was necessary to extend available methodologies to reflect the nature of these structures in a more realistic manner.

In the process of developing the above-mentioned studies, tilting simple geometry rock elements has revealed as an interesting technique that, in combination with analytical formulations can help to understand a number of issues associated to toppling phenomena. Therefore, a number of simple and a little bit more complex geometry engineered rock blocks have been tilted and results explained in this document to illustrate the potential interest of extending this technique to more realistic forms.

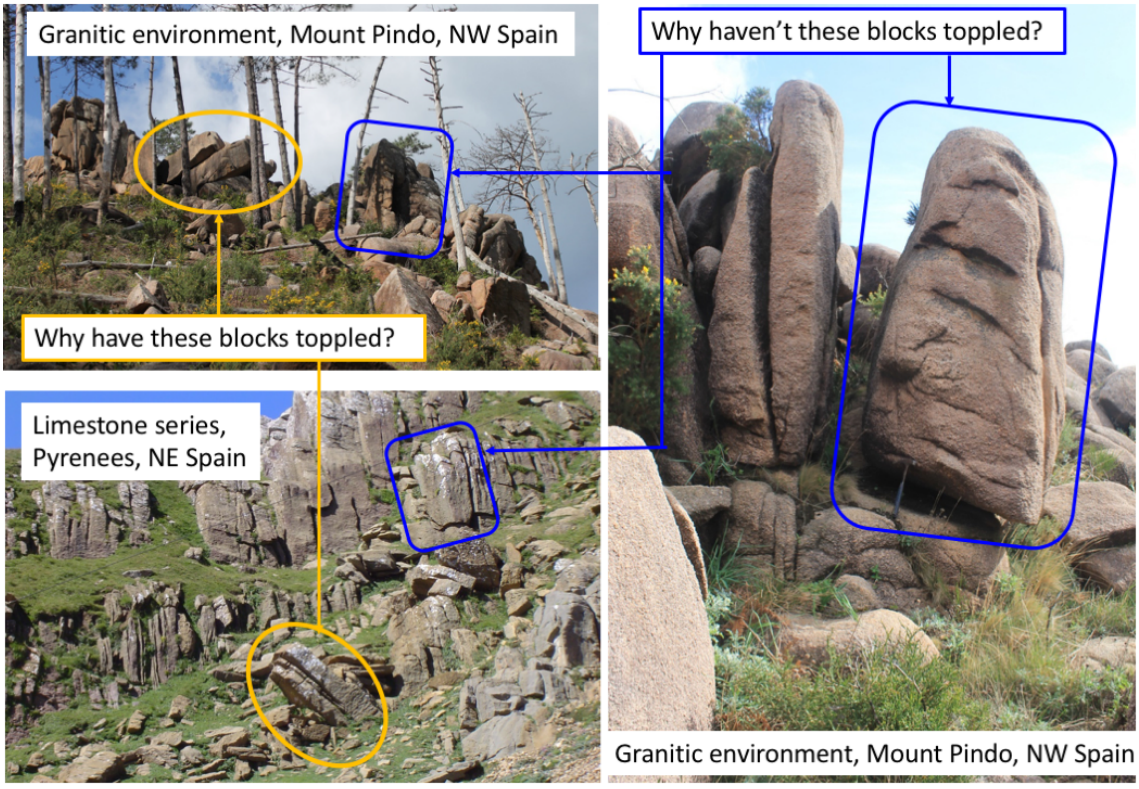

Fig. 1. Different geological environments where toppled and stable rock blocks are observed.

The study is an extension of basic toppling equilibrium calculations and was developed in parallel with particular rock slope stability studies. The initial concepts associated with the proposed methodology developed while studying the stability of wall slopes (Alejano et al., 2011) and of masonry retaining walls (Alejano et al., 2012). In both these cases it was possible to resort to physical models subjected to tilt tests in order to carry out simple analyses with the aim of confirming particular failure mechanisms and the validity of

some formulations (Fig. 2). This previously developed approach is valid if the only type of strength involved is friction and if geometry of the blocks can be easily reproduced using common rock cutting approaches (typically with saw-blades).

Fig. 2. Physical models of dry masonry retaining walls used to understand the failure mechanism of these structures and check limit equilibrium calculations.

Since the turn of the century, photogrammetric and laser scanning techniques for point cloud acquisition have become widely available, such that a very good representation of a given rock slope geometry can be achieved (Alejano et al., 2013; Armesto et al., 2009; Ferrero et al., 2011, 2009; Riquelme et al., 2014). Most recently, relatively large and accurate 3D point clouds have become available at a very reasonable cost (Girardeau-Montaut, 2018). It is therefore possible to obtain 3D point clouds representing the complex block geometries observed in nature (such as in Fig. 1). Based on such geometric data, the center of gravity (*cog*), which is critical for toppling stability analyses, can be precisely located. Other relevant geometrical aspects of the rock blocks or boulders such as the position of the contact base between the block and basal plane can be also computed rigorously. This geometrical information largely facilitates computing the factor of safety of these boulders against toppling, as the ratio of stabilizing moments to overturning moments.

Additionally, in the last five years, 3D printing has been improved so rapidly that it is relatively easy to produce a scaled 3D printed version of any rock block based on the point cloud representing its outer surface (Bader et al., 2018; Virtanen et al., 2014). This therefore allows for the possibility of using tilt testing as a methodology to analyze the stability of blocks with complex geometry against toppling.

Accordingly, in this paper we introduce a new physical modelling approach, where a tilt table, classic limit equilibrium computations, and rock physical models using a 3D-printed version of a real boulder are used to estimate the factor of safety against toppling of rock blocks in the field. It is recommended that analytical formulations or numerical models should be used in parallel with this approach to allow for a complete understanding of the relevant phenomena to be developed and to allow for possible extension of the physical modeling results to different scenarios, just as those considering the influence of water pressure or seismic loading.

2. The mechanics of toppling

Despite the fact that some authors consider the occurrence of pure toppling as an uncommon failure mechanism, and that toppling is typically associated with larger failures occurs or as a consequence of other mechanisms like slope undercutting or weakening at the toe (Hencher, 2015), toppling has been extensively reported as the origin of several rock-mass failures experienced in different fields such as open-pit mining (Alejano et al., 2010a; Al Mandalawi et al., 2019; Amini and Ardestani, 2019), civil engineering (Tu et al., 2007; Akbarpour et al., 2012; Cai et al., 2019) and natural rock slopes (Guo et al., 2017).

The mechanism of toppling had been partially identified in the field by some authors (Müller, 1968; Terzaghi, 1962), though it was not until the late 1960's (Bray, 1969) that it began to be considered as a mode of failure unto itself. A few years later, some authors started the study of toppling in a more rigorous way, through both laboratory models (Ashby, 1971; Barton, 1971) and early applications of numerical methods (Cundall, 1971; St. John, 1972).

Ashby (1971) developed a seminal study on different sliding and toppling modes of failure based on laboratory physical models and rock slopes. This author derived a simplified analytical 2-D toppling model for an isolated straight block of height h and width b, resting on a plane dipping α degrees with a friction angle between contacts, ϕ (Fig. 3).

Considering the base plane angle, $\alpha < \phi$ and the *x* and *y* components of the weight (*W*) of the block, a factor of safety against toppling can be estimated by relating the stabilizing and overturning moments with respect to the rotation pivot, P (Fig. 3a), as presented in a general form in Eq. 1.

$$FS = \frac{\sum M_{stabilizing}}{\sum M_{overturning}} \quad (1)$$

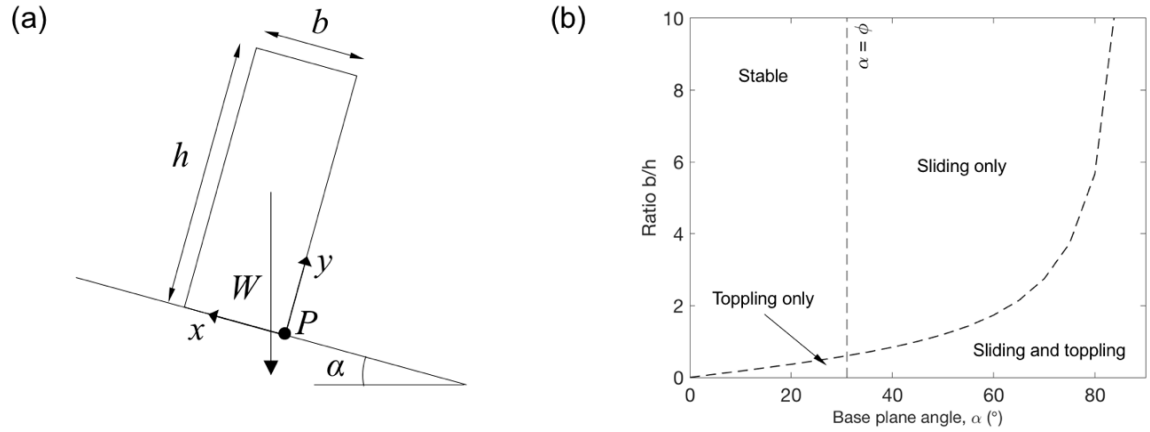

Fig. 3. (a) 2D sketch of a single block placed on an inclined plane for toppling stability analysis; (b) conditions for sliding and toppling according to Ashby (1971).

It is therefore easy to derive that the toppling condition (represented as FS ≤ 1 in Eq. 1) solely depends on the slenderness of the block and the plane dip (α) (Ashby, 1971) and is driven by the geometrical relationship presented in Eq. 2:

$$\frac{b}{h} \leq \tan \alpha \quad (2)$$

According to Fig. 3b and depending on the considered kinematic conditions stablished by Eq. 1 and the line $\alpha = \phi$, four potential conditions can be identified: stability, sliding, toppling and sliding and toppling simultaneously occurring. Even though this model laid the groundwork for subsequently reproduced studies on toppling (Hoek and Bray, 1974), some errors were detected in the conditions presented in Fig. 3b, as corrected by other

authors (Bray and Goodman, 1981; Sagaseta, 1986). The "corrected" solution for a single block toppling condition, as proposed by Sagaseta (1986), is given by Eq. 3:

$$\frac{4 \cdot \tan\alpha \cdot \left[1 + \left(\frac{b}{h}\right)^2\right] - 3 \cdot \left(\tan\alpha - \frac{b}{h}\right)}{4 \cdot \left[1 + \left(\frac{b}{h}\right)^2\right] + 3 \cdot \frac{b}{h} \cdot \left(\tan\alpha - \frac{b}{h}\right)} \leq \tan\phi \tag{3}$$

To consider the commonly observed case of rounding on the block edges caused by weathering, the single 2D straight block model was reevaluated several years later (Alejano et al., 2015). Starting from Eq. 2, the authors proposed a new equation by considering a radius of curvature (r_c) representative of the edge rounding in such a way that toppling condition is given by the geometrical relationship presented in Eq. 4:

$$\frac{b - 2r_c}{h} < \tan\alpha \tag{4}$$

It must be noted that the approaches presented above should only be applied to 2D problems or to simplifications of 3D bodies presenting the following features: constant cross-section, one dimension smaller than the other two ('thin plate' assumption), and the driving force (in this case, that corresponding to the weight of the block only) contained in the mean plane of the structure, as illustrated in Fig. 4. Additionally, the rotating pivot is already known, and defined by an identifiable edge.

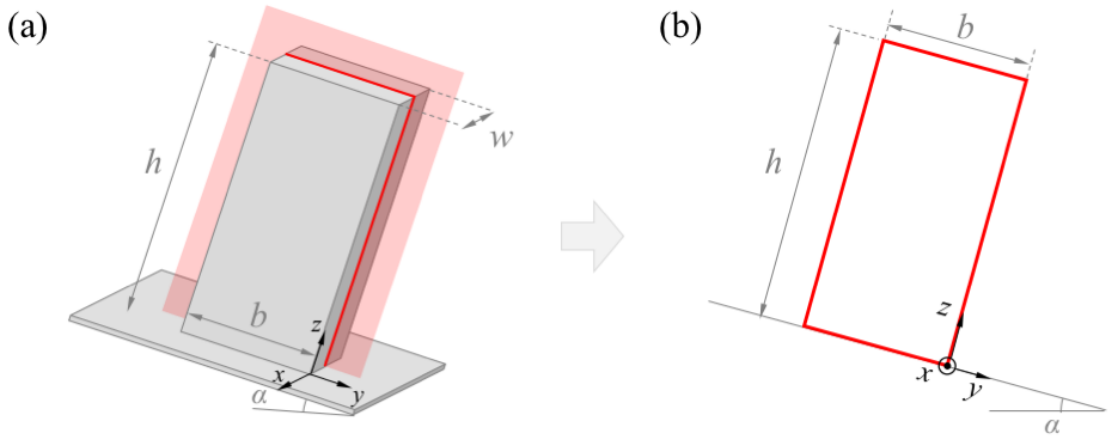

Fig. 4. (a) 3D body resting on an inclined plane with constant cross-section along the x-direction; (b) 2D simplification of the problem on the *z*–*y* plane.

Nevertheless, this situation is not commonly found in natural blocks (particularly, in rock boulders) that usually present irregular shapes and poorly defined contact planes, such that 2D analysis is unrealistic. In these cases, the third dimension cannot be disregarded and other approaches are needed for a correct assessment of the toppling mechanism (Domokos et al., 2012; Yeung and Wong, 2007; Zábranová et al., 2020).

3. Analytical assessment and laboratory physical modelling

An experimental program was designed in order to study the critical angle of toppling of single engineered models subjected to tilt tests under laboratory conditions. The idea was to test different blocks or assemblies presenting features that determine their kinematic behavior with respect to toppling: the symmetry of the block section, the edge rounding, the concavity of the contact base and the position of the center of gravity with respect to a central cross-section of the block. A sketch showing these features and the models used is presented in Fig. 5.

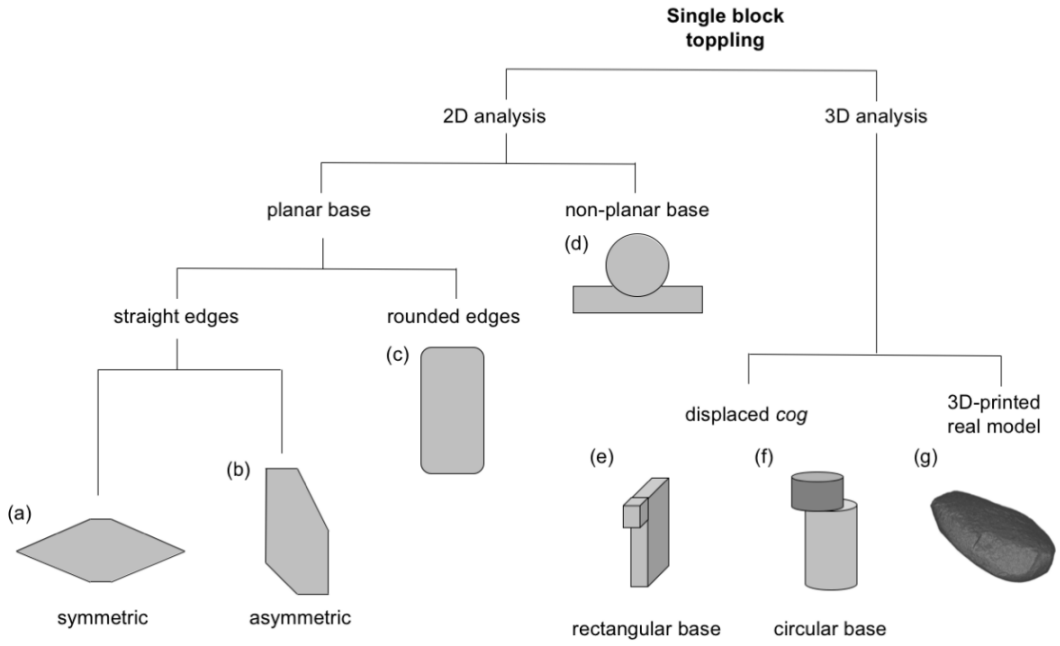

Fig. 5. Sketch showing the specimens used for 2D and 3D toppling analyses according to the type of contact base (planar or non-planar), edge rounding (straight or rounded), symmetry of the cross-section and position of the *cog*.

3.1. Physical models and laboratory testing

The models presented in Fig. 5 were selected to perform the laboratory tilt tests. The majority of them (Fig. 5 a–e) consisted of some saw-cut pieces of two igneous rocks (granite and orthogneiss) assembled by gluing them together to form the physical model (Fig. 6). A photo of each model is presented in Fig. 7. In mode case PM-6 (Fig. 5f and Fig. 7e), steel (with a density of 7900 kg/m^3) was used to fabricate the upper cylinder; as can be appreciated, this part of the model was intended to displace the center of gravity of the corresponding assembly. The replica of a real boulder was 3D-printed with PLA (polylactide) plastic based on a 3D point cloud recovered from the original geological structure (Pérez-Rey et al., 2019).

The density of the plastic is lower than that of the rock. Additionally, the printed version presents an internal plastic pattern with regular hollow zones. Since toppling stability depends in both the stabilizing and overturning moments and they are both proportional to the block weight, density does not influence stability in uniform bodies. The friction in the base is also proportional to the weight in case the contact is considered planar, though it may affect results for rough joints, as the Barton's formula suggest. Since the contacts of the studied elements are typically planar, the weight does not significantly affects the frictional response. When we want to avoid the sliding mechanism, in cases where it can take place at lower tilt angles than toppling, a piece of sand paper can be glued to the base of the element. In conclusion, density, when constant, and friction angle are considered to have a negligible impact on the presented results.

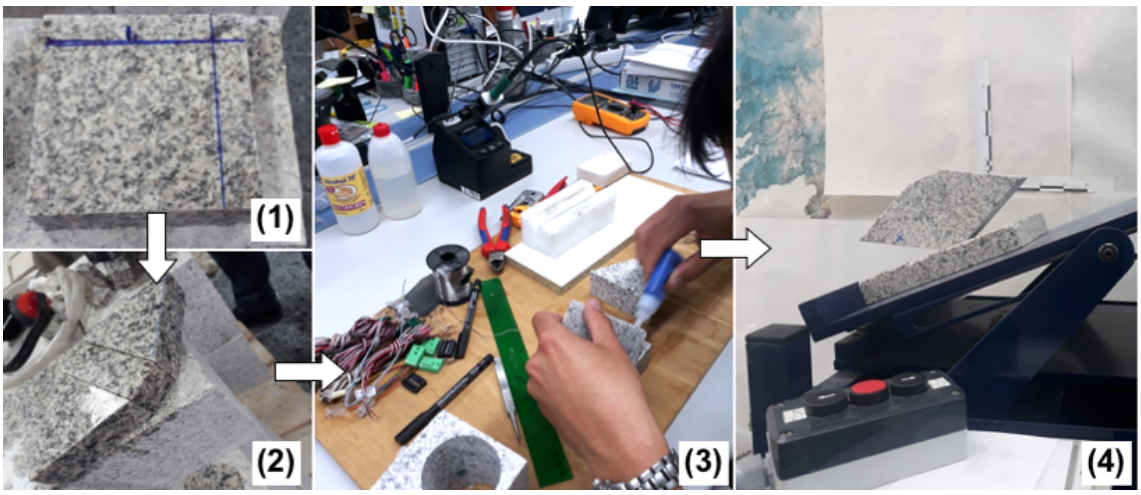

Fig. 6. Process of fabrication of the rock models (1, 2) dimensioning and parts of a model; (3) gluing of parts to create the complete model and (4) model being tested.

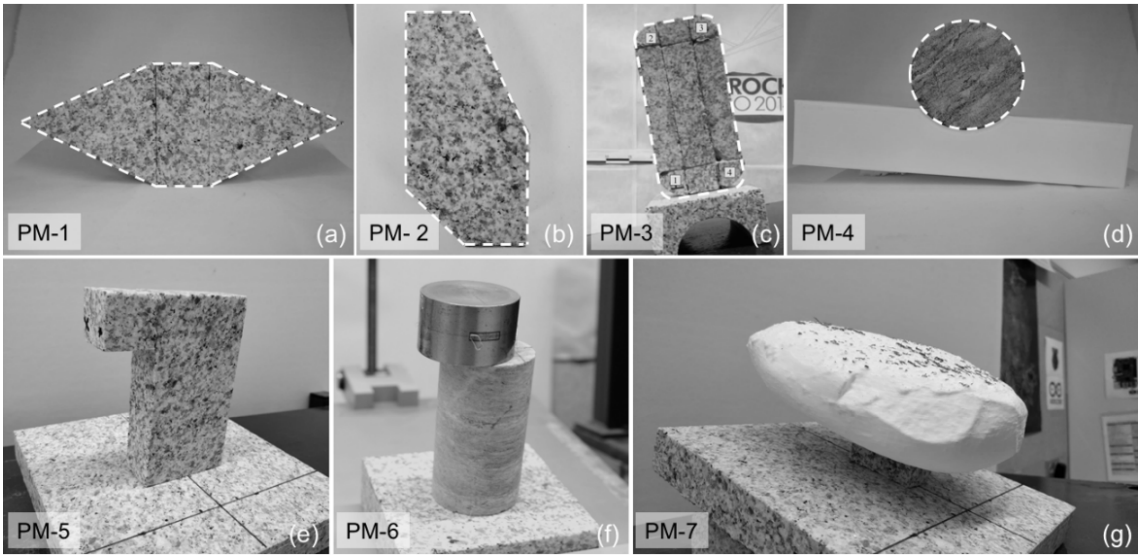

Fig. 7. Photos of the physical models used in this study (a. symmetric section; b. asymmetric section; c. rounded edges; d. concave base; e. displaced *cog* (rectangular base); f. displaced *cog* (circular base); g. 3D printed replica of a real boulder). The name assigned to each model is also provided.

Regarding the tilt tests, they were carried out with a custom testing frame designed at the University of Vigo that consists of a metallic platform able to rotate about a fixed axis and driven by an asynchronous motor that constant angular lifting velocities (from 0.1º/min to 26º/min) to be maintained. The 'start' and 'stop' orders can be given to the machine by a manual control. A constant record of the tilting angle is kept using an inclinometer (*Leica DISTO D5*) with an accuracy of 0.1º attached to the platform (Fig. 8). The critical angle of toppling for each tested model could be registered by simply stopping the rotation of the platform when the onset of instability was observed. For that purpose, the lifting velocity was set at 12º/min for all tests in order to balance precision in determination of the critical angle with testing time. Each model was tested three times until toppling occurred, and results were collected for purposes of comparison with analytical and numerical predictions.

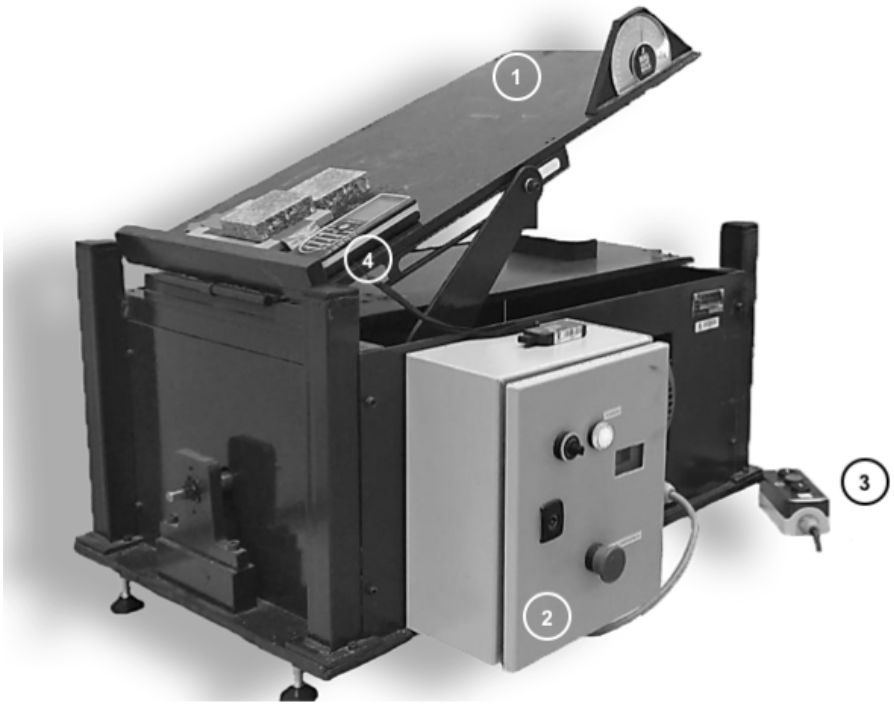

Fig. 8. Tilting platform used for carrying out tilt tests with the physical models (1. rotating platform; 2. connection box and velocity control; 3. 'start and stop' control; 4. digital inclinometer).

3.2. Analytical assessment of toppling

With the models PM-1 to PM-4 presented in Fig. 5, it is possible to develop simple 2D analytical predictions of the critical angle of toppling. To do that, some cross-sections were divided into simpler shapes (like squares, rectangles and triangles). The driving forces were located at the centroid of each subsection and the stabilizing and overturning moments were calculated by considering the rotation pivot as the lower corner of the model in contact with the tilting table, which was also set as the origin of the coordinate system for calculations. The critical angle of toppling, α_{cr}, can easily be estimated by imposing a factor of safety, FS = 1 in Eq. 1.

Other scenarios like those presented for models PM-5 to PM-7 require a more detailed analysis on the positioning of the *cog* as well as the rotation pivot.

It is relevant to note that the relative stability of any of the blocks under scrutiny for any position can be both computed in terms of factor of safety and in terms of critical stability angle. Obviously, these two approaches are related to one another, so they can be

computed for different scenarios. For test interpretation purposes where no additional forces exist (water, earthquakes), the authors have selected the critical angle approach, thinking it could be more illustrative for output comparison purposes. However, a factor of safety approach could also be developed.

3.2.1. Symmetric model with straight edges and planar base

The simplest model studied (PM-1), in terms of geometry, consists of a symmetric block with a constant cross-section that can be divided in two triangles and a rectangle. The model is defined in terms of the central block breadth, *b*. A sketch of this model is presented in Fig. 9, where the relevant force components and the rotation pivot are also indicated for a given inclination of the base (α).

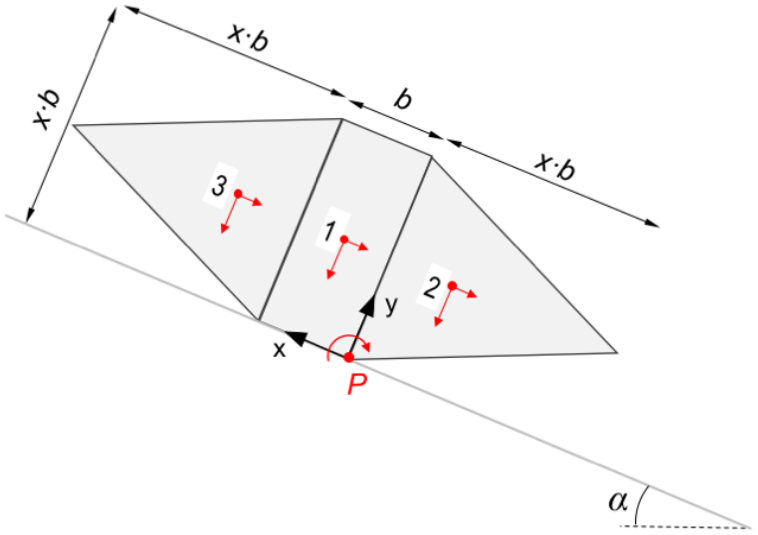

Fig. 9. Sketch of the symmetric model with constant cross-section, where the centroid of each sub-element is shown as well as the rotation pivot and origin of x-y coordinates.

For demonstrative purposes, we present the derivation of the critical angle formulation, based on the computation of the factor of safety for the rock block illustrated in Fig. 9. If one considers the rotation pivot (P) as the origin, the expression for estimating the factor of safety (*FS*) dividing the block in its three basic elements is as follows:

$$FS = \frac{\sum M_{stabilizing}}{\sum M_{overturning}} = \frac{W_1 \cos\alpha \, \frac{b}{2} - W_2 \cos\alpha \, \frac{xb}{3} + W_3 \cos\alpha \, \frac{(3+x)b}{3}}{W_1 \sin\alpha \, \frac{xb}{2} + W_2 \sin\alpha \, \frac{xb}{2} + W_3 \sin\alpha \, \frac{xb}{2}} \quad (5)$$

In this case, all forces acting parallel to the x-axis correspond strictly to destabilizing moments, while those acting parallel to the y-axis contribute to both the stabilization (sub-sections 1 and 3) and destabilization (sub-section 2) of the block shown in Fig. 9.

Accounting for the fact that $W_2 = W_3$, and that $W=W_1+W_2+W_3$, Eq. 5 can be simplified to:

$$FS = \frac{\sum M_{stabilizing}}{\sum M_{overturning}} = \frac{W \cos\alpha \, \frac{b}{2}}{W \sin\alpha \frac{xb}{2}} = \frac{1}{x \cdot \tan\alpha} \quad (6)$$

Equating the *FS* to 1, the point at which instability initiates, the critical angle for toppling in Fig. 9 can be derived as Eq. 7:

$$\alpha_{cr} = \operatorname{atan}\left(\frac{1}{x}\right) \quad (7)$$

This implies that, as mentioned above, the size of the sample does not influence results, so the physical model represents the behavior of any smaller or larger homothetic block. For the analyzed case and taking into account that $x = 2.7$, the critical angle in this case will be $\alpha_{cr} = 20.32º$ as derived from Eq. 7. The influence of the acuteness of the lateral triangle parts could be easily computed by testing different values of x in Eq. 7. This kind of analytical solution is therefore quite favorable for evaluation of the influence of some geometrical parameters of the blocks under scrutiny.

Alternatively, the *FS* can be computed for the case the *cog* is known from the beginning accounting for the stabilizing and overturning moments of the weight as presented in Eq. 1. For blocks with more complex geometry, it therefore tends to be most convenient to compute the position of the *cog* to simplify subsequent computations.

3.2.2. Asymmetric model with straight edges and planar base

This model (named as PM-2) presents an asymmetric cross-section that can be divided into simpler shapes (i.e. two rectangles and two triangles) to simplify calculations, as presented in Fig. 10.

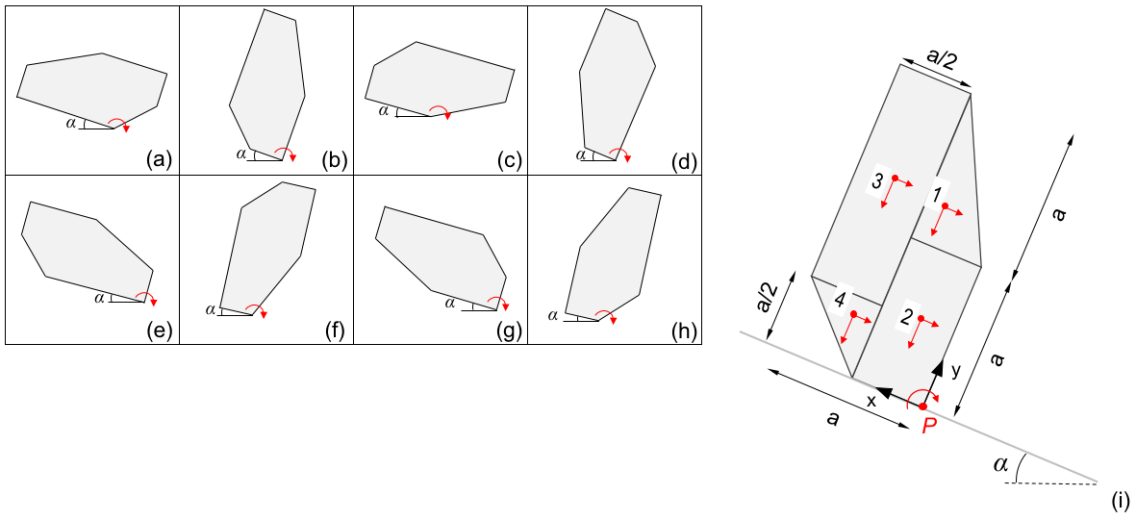

Fig. 10. Sketch of an asymmetric model with constant cross section and straight edges. All the possible testing positions for toppling analyses are presented (a-h). The sub-sections (1-4) indicated in the enlarged sketch (i) on the left are kept for all models.

For the model sketched in Fig. 10i (equivalent to that in Fig. 10b), the angle of critical toppling can be estimated with Eq. 8, in which the cross section was divided in four simpler subsections.

$$\alpha_{cr} = \arctan\left(\frac{W_1\frac{a}{3} + W_2\frac{a}{4} + W_3\frac{3a}{4} + W_4\frac{2a}{3}}{W_1\frac{4a}{3} + W_2\frac{a}{2} + W_3\frac{5a}{4} + W_4\frac{a}{3}}\right) \quad (8)$$

By modifying the position of the PM-2 block as presented in Fig. 10i, it is possible to get different scenarios that will change the cross section to be analyzed, as shown in Fig. 10a-h and, consequently, the critical angle of toppling. This procedure is valuable when performing the experimental part of the present work, since it will allow testing a single model in eight different positions.

To illustrate how the stability against toppling and, ultimately, the critical angle of this relatively complex geometry block could be computed, the complete set of equations (Eq.

9-16) for calculating the analytical critical angle of toppling for each position of the block is presented in Table 1. Again, in this case, as in any other, the stability against toppling will be completely independent of the block size.

Table 1. Equations for estimating the FS against toppling and angles of critical toppling for all the positions presented in Fig. 10 (a-h).

Block position	Equation	
(a)	$\alpha_{cr} = \arctan\left(\frac{W_1 \cdot \frac{5a}{6} + W_3 \cdot \frac{3a}{4} - W_4 \cdot \frac{a}{6}}{W_1 \cdot \frac{2a}{3} + W_2 \cdot \frac{3a}{4} + W_3 \cdot \frac{a}{4} + W_4 \cdot \frac{a}{3}}\right)$	(9)
(b)	$\alpha_{cr} = \arctan\left(\frac{W_1 \cdot \frac{a}{3} + W_2 \cdot \frac{a}{4} + W_3 \cdot \frac{3a}{4} + W_4 \cdot \frac{2a}{3}}{W_1 \cdot \frac{4a}{3} + W_2 \cdot \frac{a}{2} + W_3 \cdot \frac{5a}{4} + W_4 \cdot \frac{a}{3}}\right)$	(10)
(c)	$\alpha_{cr} = \arctan\left(\frac{-W_1 \cdot \frac{a}{3} + W_2 \cdot \frac{a}{2} - W_3 \cdot \frac{a}{4} + W_4 \cdot \frac{2a}{3}}{W_1 \cdot \frac{a}{3} + W_2 \cdot \frac{a}{4} + W_3 \cdot \frac{3a}{4} + W_4 \cdot \frac{2a}{3}}\right)$	(11)
(d)	$\alpha_{cr} = \arctan\left(\frac{W_1 \cdot \frac{2a}{3} + W_2 \cdot \frac{3a}{4} + W_3 \cdot \frac{a}{4} + W_4 \cdot \frac{a}{3}}{W_1 \cdot \frac{2a}{3} + W_2 \cdot \frac{3a}{2} + W_3 \cdot \frac{3a}{4} + W_4 \cdot \frac{5a}{3}}\right)$	(12)
(e)	$\alpha_{cr} = \arctan\left(\frac{W_1 \cdot \frac{2a}{3} + W_2 \cdot \frac{3a}{2} + W_3 \cdot \frac{3a}{4} + W_4 \cdot \frac{5a}{3}}{W_1 \cdot \frac{2a}{3} + W_2 \cdot \frac{3a}{4} + W_3 \cdot \frac{a}{4} + W_4 \cdot \frac{a}{3}}\right)$	(13)
(f)	$\alpha_{cr} = \arctan\left(\frac{-W_1 \cdot \frac{a}{6} - W_2 \cdot \frac{a}{4} + W_3 \cdot \frac{a}{4} + W_4 \cdot \frac{a}{6}}{W_1 \cdot \frac{2a}{3} + W_2 \cdot \frac{3a}{2} + W_3 \cdot \frac{3a}{4} + W_4 \cdot \frac{5a}{3}}\right)$	(14)
(g)	$\alpha_{cr} = \arctan\left(\frac{W_1 \cdot \frac{4a}{3} + W_2 \cdot \frac{a}{2} + W_3 \cdot \frac{3a}{4} + W_4 \cdot \frac{a}{3}}{W_1 \cdot \frac{a}{3} + W_2 \cdot \frac{a}{4} + W_3 \cdot \frac{3a}{4} + W_4 \cdot \frac{2a}{3}}\right)$	(15)
(h)	$\alpha_{cr} = \arctan\left(\frac{W_1 \cdot \frac{a}{6} + W_2 \cdot \frac{a}{4} - W_3 \cdot \frac{a}{4} - W_4 \cdot \frac{a}{6}}{W_1 \cdot \frac{4a}{3} + W_2 \cdot \frac{a}{2} + W_3 \cdot \frac{5a}{4} + W_4 \cdot \frac{a}{3}}\right)$	(16)

3.2.3. Symmetric model with rounded edges and planar base

Another model presenting a symmetric cross-section is that corresponding to a rectangular prism with rounded corners (PM-3), as originally analyzed by Alejano et al. (2015). The cross-section of the model is shown in Fig. 11 and, due to the simplicity of this section, only the *cog* of the entire model was considered.

If the moment equilibrium calculation is performed for the model presented in Fig. 11, the angle of critical toppling can be estimated (Eq. 17) as rearranged from Eq. 4. Note that the addition of a non-zero radius of curvature (r) reduces the critical angle of toppling, since it diminishes the actual contact width by $2r_c$.

$$\alpha_{cr} = \arctan\left(\frac{b - 2r_c}{h}\right) \tag{17}$$

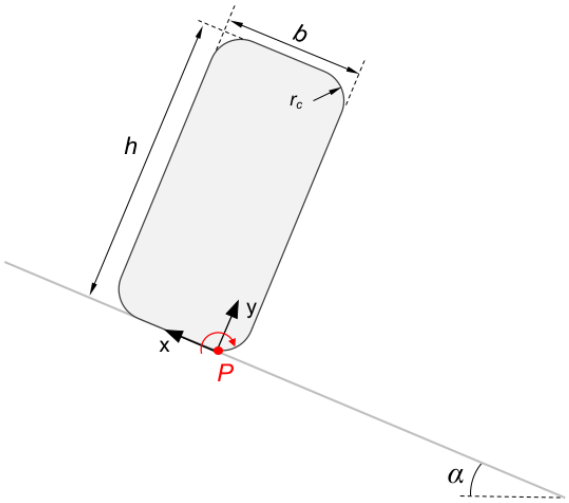

Fig. 11. Sketch of the symmetric model with rounded edges (for the studied model: h/b = 2.125 and r_c/h = 0.147).

3.2.4. Model with non-planar (concave) base

The present model is intended to illustrate the effect of a non-planar (concave) base, as a potentially stabilizing factor. The idea was to study a circular cross-section in which part of it is embedded in the inclined plane, resting on a concave base that coincides with the curvature of the cross section (see Fig. 7b and Fig. 12).

It can be demonstrated that the angle of critical toppling, α_{cr}, of the model presented in Fig. 12 solely depends on the depth of the slot (s) relative to the radius of the circular cross-section (r), n, where $n = s/r$ for and $n \in (0, 1)$. The angle of critical toppling can therefore be calculated from Eq. 18.

$$\alpha_{cr} = \operatorname{atan}\left\{\frac{\sin[\operatorname{acos}(1 - n)]}{1 - n}\right\} \tag{18}$$

With the aim of illustrating the effect of a concave contact on the angle of critical toppling of such a circular section of radius *r*, the critical angle is plotted against the depth of the slot expressed as a proportion of the radius (*n*) in Fig. 13.

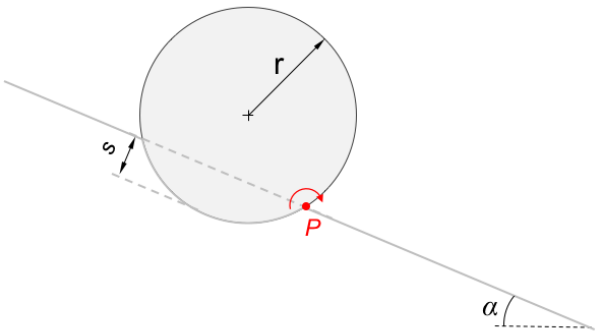

Fig. 12. Sketch of the model with non-planar (concave) base.

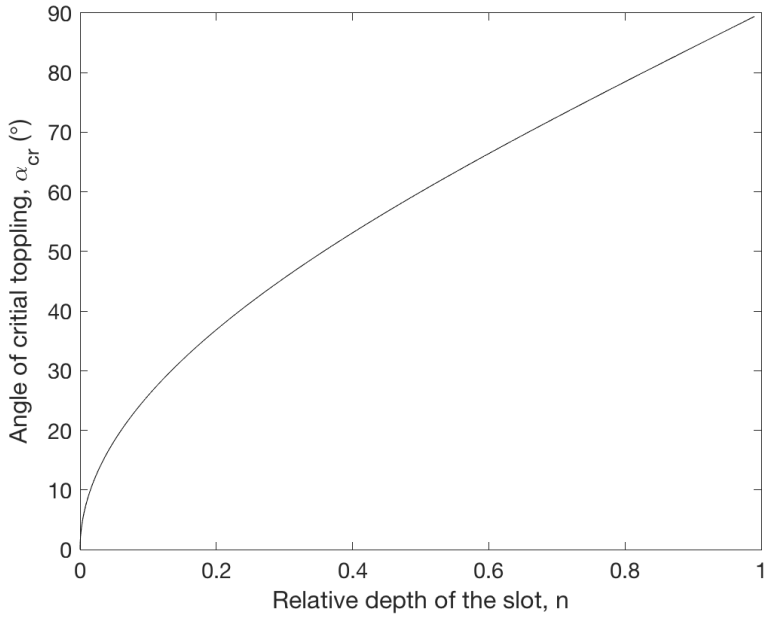

Fig. 13. Dependence of the angle of critical toppling (y-axis) with the relative depth of the slot, n (x-axis), for the model depicted in Fig. 12.

As is shown in Fig. 13, the effect of a concave contact clearly influences the angle of critical toppling of a block with a circular section. This effect is most significant for low values of *n*, where the derivative $d\alpha_{cr}/dn$ is maximized; while almost no blocks are expected to match the geometry shown in Fig. 12 perfectly, in practice, this means that even relative small degree of concavity in the basal plane for a block of more general shape has the potential to increase the angle of critical toppling by a few degrees.

3.2.5. Model with the *cog* not contained in a symmetry plane: squared/rectangular base

The position of the center of gravity (*cog*) or centroid clearly influences the toppling behavior of an element as in the case of the blocks already analyzed in this study. If a block is positioned onto a flat surface and the vertical projection of its *cog* falls inside the contact area, the block will remain stable against toppling. Consider the situation illustrated in Fig. 14a for a squared-based, symmetric and homogeneous block. In this case, if the *cog* is projected onto the planar base, that projection will fall on the center of the square section. If the block is progressively tilted, it will topple once the projection of the *cog* falls out the base.

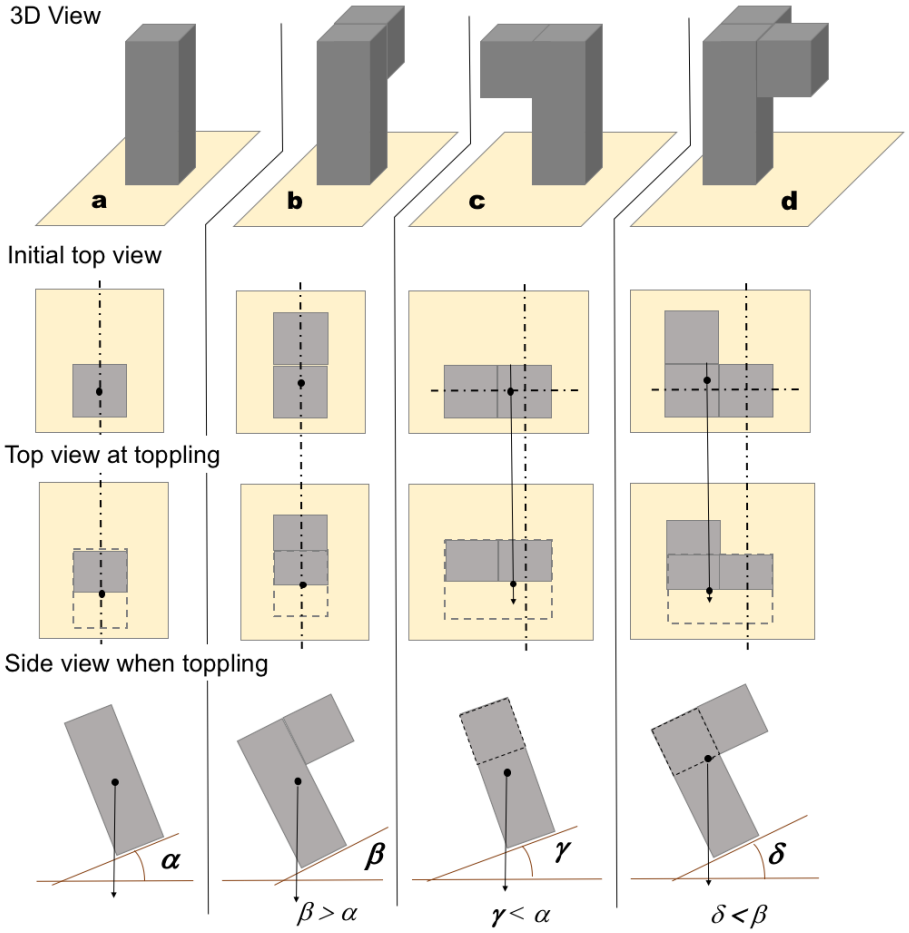

Fig. 14. Different 3D elements (a, b, c and d) to be subjected to a tilt test to illustrate the role of geometry on toppling. On the upper row, 3D view of the elements resting on a horizontal base to be tilted. On the second row, initial top view with the projection including the *cog*. On the third row, top view of the surface after tilting and in the moment of toppling and, on the last row, side view of platform and element when toppling.

Fig. 14b shows a similar prism with a cube stuck to its upper back face, a more complex geometry. The *cog* of this model, when placed on a flat surface, will not project on the center of the base but will instead project somewhere behind the center of the base due to the added mass. Because of this, when tilting the plane where this element stands, it will topple at a higher angle than the previous case; in other words, the angle of critical toppling in this case (α) will be higher than the one observed for the element shown in Fig.14a (β).

The third element (Fig. 14c) is similar to element 'b', but the added cube is now stacked on the upper part of a lateral face. Its *cog* will be at the same height as for element b (since it is the same element in the same position), but its projection onto a horizontal plane will be moved to the left in relation to element 'a' (Fig. 14c, second row). When tilting the platform where element 'c' rests, it will topple at a lower angle than α, because its *cog* is located higher than in case 'a', meaning its projection will fall outside its base at a lower angle γ, which will be also less steep than β.

Element 'd' is a rectangular prism with a square cross-section where two cubes are attached on the upper part of its lateral backward and leftward faces. In this case, the *cog* of the element will be even more displaced upwards than in the case of elements 'b' and 'c' and the *cog* projection on its base will be slightly moved backwards and a little bit to the left in relation to the case of element 'a' in Fig 14. This will clearly be less stable than 'b' (since the side-stuck cubes displace the *cog* upwards) but more stable than 'c' (since the back-stuck cube will increase its stability by moving the projection of its *cog* backwards). According to the previous analyses, a hierarchy on the angle of critical toppling can be stablished for the studied models shown in Fig. 14 as: $\beta > \delta > \alpha > \gamma$.

With the goal of assessing the effect of a displaced *cog* on the toppling behavior in a more detailed way and following the ideas described in the previous paragraph, the model presented in Fig. 15 has been considered. It consists of a rectangular-based block with a small prismatic slab stuck on the upper part of a lateral face (see Fig. 15b.1).

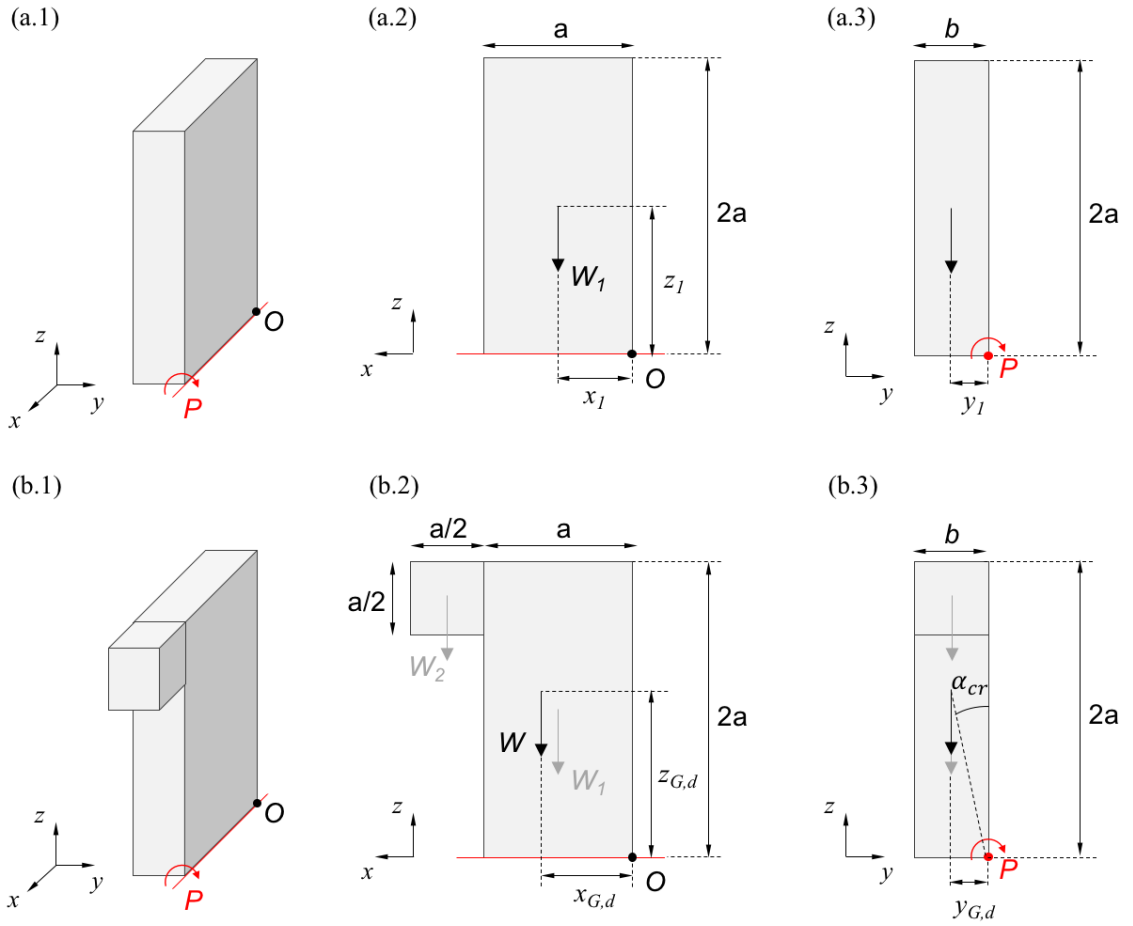

Fig. 15. (a) 3D view of the model with the axis of rotation and origin of coordinates for positioning the *cog* marked; (b) levelled front view of the assembly and (c) levelled lateral view of the assembly.

As previously mentioned, the effect of adding such a piece to a rectangular-based block as shown in Fig. 15 implies a displacement of the *cog*, which will move towards the added mass. This positioning of the *cog* can be easily determined by resorting to Eqs.19, 20 and 21 for each coordinate, respectively, when considering $m_i = W_i / g$.

$$x_{G,d} = \frac{\sum(m_i \cdot x_i)}{\sum m_i} \tag{19}$$

$$y_{G,d} = \frac{\sum(m_i \cdot y_i)}{\sum m_i} \tag{20}$$

$$z_{G,d} = \frac{\sum(m_i \cdot z_i)}{\sum m_i} \tag{21}$$

Once the 3D coordinates of the displaced *cog* are set ($x_{G,d}$, $y_{G,d}$, $z_{G,d}$), the angle of critical toppling for the model sketched in Fig. 13b.1 can be estimated using Eq. 22:

$$\alpha_{cr} = \text{atan}\left(\frac{y_{G,d}}{z_{G,d}}\right) \tag{22}$$

It has to be highlighted that all the models with a rectangular or squared-base such as those shown in the previous sections and particularly the last shown in Fig. 15 will always have a pre-defined axis of rotation, which coincides with an edge of the block in contact with the rotating base. This is not the case for circular or irregular-based specimens, as considered in Section 3.2.6.

3.2.6. Model with the *cog* not contained in a symmetry plane: circular base

Real rock blocks and boulders as found in the field rarely have a *cog*s that project onto the centers of their bases when resting on horizontal surfaces, nor do they have well-defined axes of rotation against toppling mechanism due to their typically irregular shapes. As already noted, for a precise assessment of their stability against toppling, it will be necessary to correctly position the *cog* as well as the pivot or axis around which the toppling mechanism will take place.

The study of these features has been carried out using a laboratory physical model (as shown in Fig. 7f) consisting of two cylinders composed of different materials (rock and steel with densities of ρ_r = 2700 kg/m^3 and ρ_s = 7800 kg/m^3, respectively). Both cylinders have the same radius (r = 27 mm) but different heights, with the rock cylinder measuring 100 mm in height and the steel cylinder measuring 35 mm in height. The assembly is sketched in Fig. 16b.1.

This test consisted of placing the two specimens as shown in Fig. 16b.1, with the top piece moved outwards a distance of r/2. This position of the top steel specimen moves the center of gravity out of the plane of symmetry of the lower specimen, as can be seen in the front view shown in Fig. 7b. Then, the specimen was progressively tilted (being the platform rotation around the x-axis) until toppling of the entire set occurred, when the tilting angle (angle of critical toppling) was achieved.

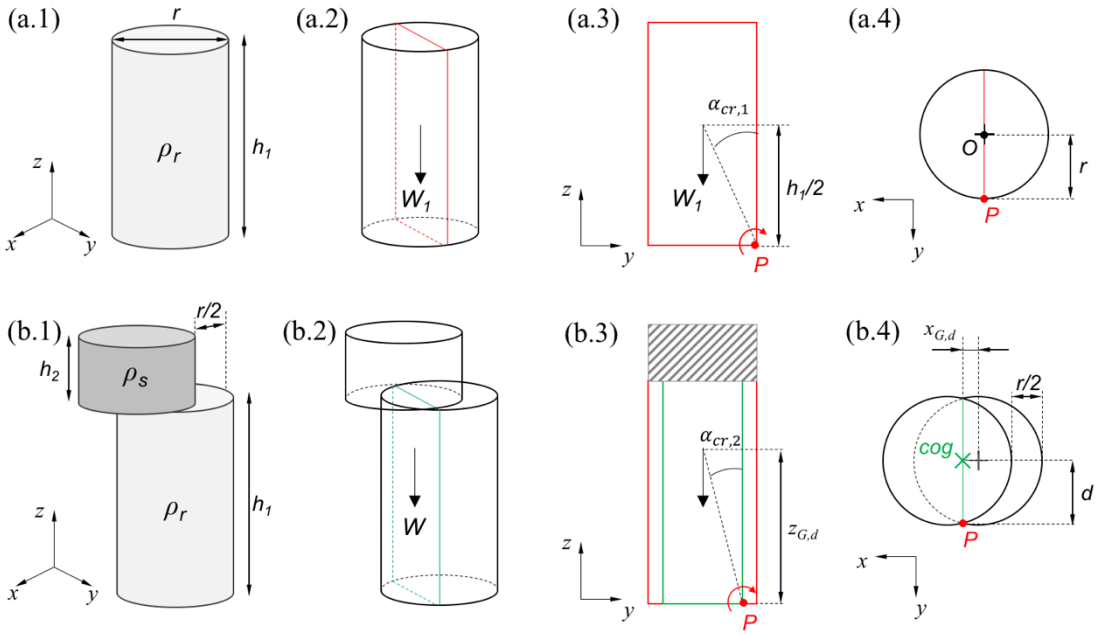

Fig. 16. Different views of the model containing the *cog* out of a symmetry axis (model PM-6).

By considering the origin of the coordinate system at the center of the base of the lower cylinder (Fig. 16a.4) the angle of critical toppling for the model presented in Fig. 16b.1 when tilted around the x-axis can be calculated using Eq. 23:

$$\alpha_{cr} = \text{atan}\left(\frac{d}{z_{G,d}}\right) \tag{23}$$

Unlike the other examples considered in this study, this model will behave differently once the limit equilibrium for toppling has been reached. Specifically, although the critical angle of toppling can be calculated in a similar way to that of the other models (Eq. 12), the reduction of the cross-section (plane) containing the *cog* of the assembly (shown in green in Fig. 16b.3 and Fig. 16b.4) has to be considered, as it influences the axis of rotation.

As shown in Fig. 17, the axis (pivot) of rotation will not coincide with that of the rotating platform and will move laterally due to the displacement of the *cog* and the circular base in such a way that the new axis of rotation corresponds to the tangent at the intersection point between the plane containing the new *cog* (shown in green color in Fig. 17) and the base of the model. The displacement angle, δ, as shown in Figure 17 can be calculated using Eq. 24.

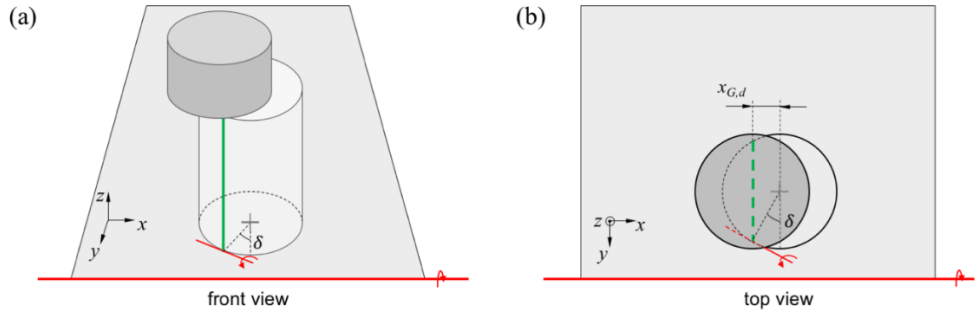

Fig. 17. Different views of the model PM-6 at the equilibrium limit state, where the axis of rotation does not coincide with that of the rotating platform.

$$\delta = \operatorname{asin}\left(\frac{x_{G,d}}{r}\right) \tag{24}$$

3.2.7. 3D-printed model representative of a real boulder

The last model (PM-7) considered in this study corresponds to a plastic (PLA) replica of a real granitic boulder located in the NW of Spain, as studied by Pérez-Rey et al. (2019). The replica, made at a scale of approximately 1:50, was created from an 3D point cloud of the real boulder collected in the field, which was afterwards processed with the software *CloudCompare* (Girardeau-Montaut, 2018) and *Meshlab* (Cignoni et al., 2008) in order to develop the 3D printing stage with a *BCN Sigma 3D* printer (see Fig. 18).

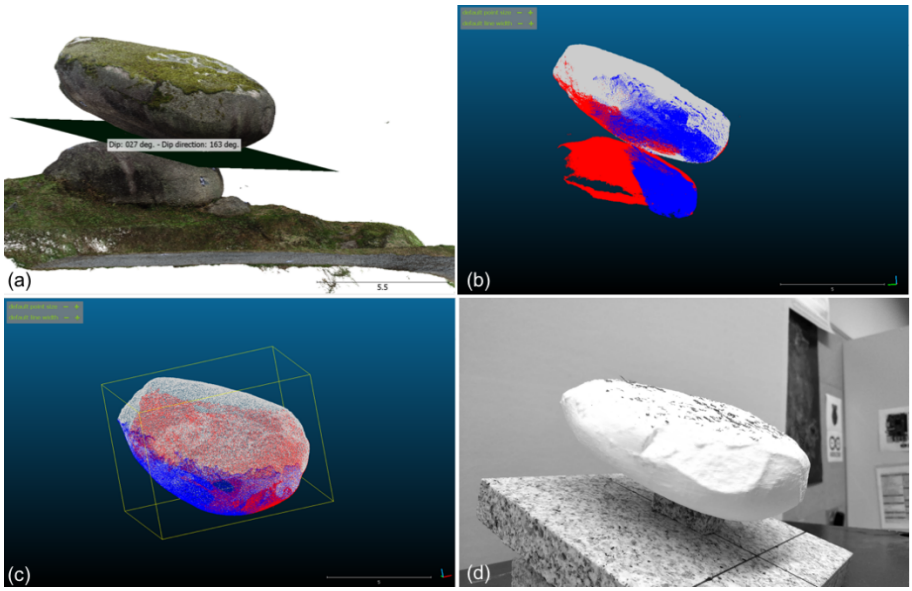

Fig. 18 (a, b) Two views of the 3D point cloud of the studied boulder; (c) isolation of the boulder from the rest of the structure and (d) 3D-printed replica on the testing platform.

By taking advantage of such a precise 3D point cloud and with the assistance of *CloudCompare* software, it is possible to approximate, in a reasonable manner, the contact area between the boulder and the base and to position the *cog*.

Using the relationship presented by Eq. 23 and the geometrical parameters presented in Fig. 19, it is possible to estimate the approximate angle of critical toppling of the boulder to be $\alpha_{cr} = 31.4°$.

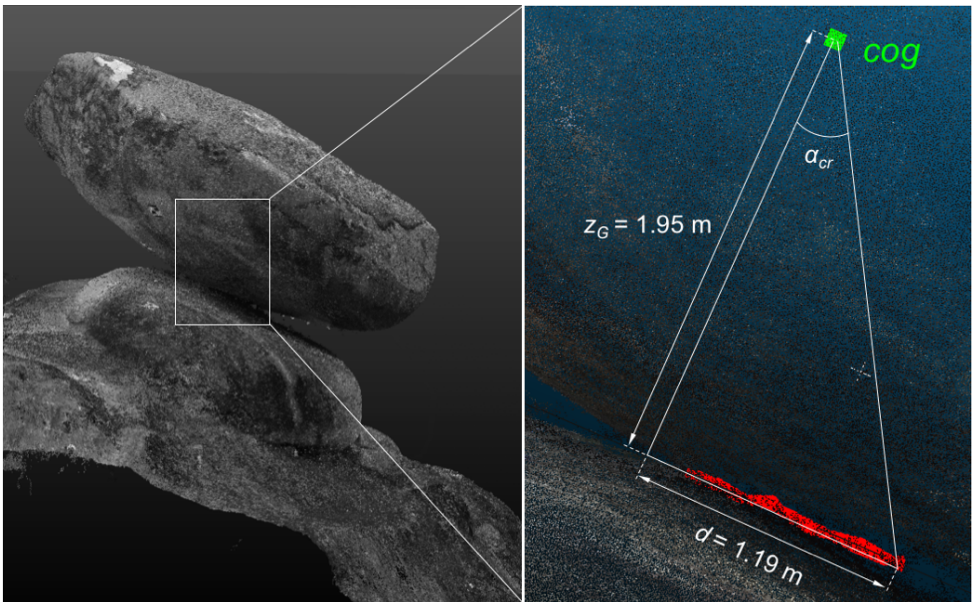

Fig. 19. Detailed view of the position of the *cog* projected onto the contact plane, showing the distance *d* necessary for estimating the critical angle of toppling.

4. Results

4.1. Comparison of analytical and experimental results

After carrying out all calculations of the angle of critical toppling of each of the models considered for this study, as presented in Section 3, all analytical results are shown in Table 1. Together with these results, the experimental angles of toppling obtained for each series of three tests carried out with the seven models are also provided with an averaged result. As it can observed in this table, the discrepancy of the analytical and average laboratory results is always less than 1.3º, and the median error is 0.66º.

It must be noted that some models did not achieve toppling failure in the laboratory tests (in particular, the PM-2 model in some positions). This occurs when the theoretical toppling angle is greater than the basic friction angle of the base contact surface, so the block slides before reaching its toppling angle. These results are indicated in Table 2 with an ‘s’. It has also been observed that PM-2 model in position (h) was not self-stable in a horizontal position ($\alpha_{cr} < 0$).

Table 2. Analytical and experimental results for the angle of critical toppling as obtained for the seven studied models.

Model	Position	Analytical	Experimental (s = slide)			
		α_{cr} (°)	α_1	α_2	α_3	α_{mean}
PM-1	—	20.32	20.2	20.3	20.5	20.3
PM-2	(a)	44.22	30.4 (s)	27.2 (s)	30.1 (s)	29.2 (s)
	(b)	28.66	29.1	29.0	29.2	29.1
	(c)	4.18	3.2	3.2	3.1	3.2
	(d)	24.55	25.4	25.3	25.6	25.4
	(e)	65.45	33.5 (s)	30.9 (s)	27.0 (s)	30.5 (s)
	(f)	1.41	2.6	2.7	2.7	2.7
	(g)	61.34	29.0 (s)	25.6 (s)	26.5 (s)	27.0 (s)
	(h)	< 0	—	—	—	—
PM-3	—	10.01	11.0	11.0	9.67	10.6
PM-4	(a) (n =1/6)	33.56	33.3	32.5	32.8	32.9
	(b) (n=1/3)	48.19	47.3	48.3	48.4	48.0
PM-5	—	11.88	11.6	12.3	12.4	12.1
PM-6	—	17.29	16.5	15.9	16.2	16.2
PM-7	—	31.39	30.8	30.4	30.7	30.6

4.2. 3D discrete numerical modelling

Another way to validate the results of the physical models is by comparing these results with those obtained by numerical analysis. For this part of the study, we have utilized the Distinct Element Method (DEM), which applies an explicit finite difference method for modelling large displacements and rotations of block systems (Cundall, 1971). This method has been used in numerous studies of toppling (Brideau and Stead, 2010; Lanaro et al., 1997; Pritchard and Savigny, 1990). In this case, we use the DEM as implemented in the software 3DEC v5.20 (Itasca Consulting Group, 2019).

Discrete Element Methods can deal with geological structures of any size and shape, and with a great variety of constitutive models for both the intact rock and the discontinuities. They also allow for simulation of complex hydrogeological environments or time-dependant phenomena like rock-dynamics or creep. In this study, this approach was used because it does not require the prior definition of a displacement direction (as required in the analytical calculation), meaning the results of the other methods can be confirmed in

628 cases where there is any doubt about the displacement direction, such as for models with
629 a displaced *cog* (PM-5 and PM-6), or the model with an irregular and complex shape
630 (PM-7). The same tilt tests performed with the physical models were simulated in 3DEC
631 (Fig. 20).

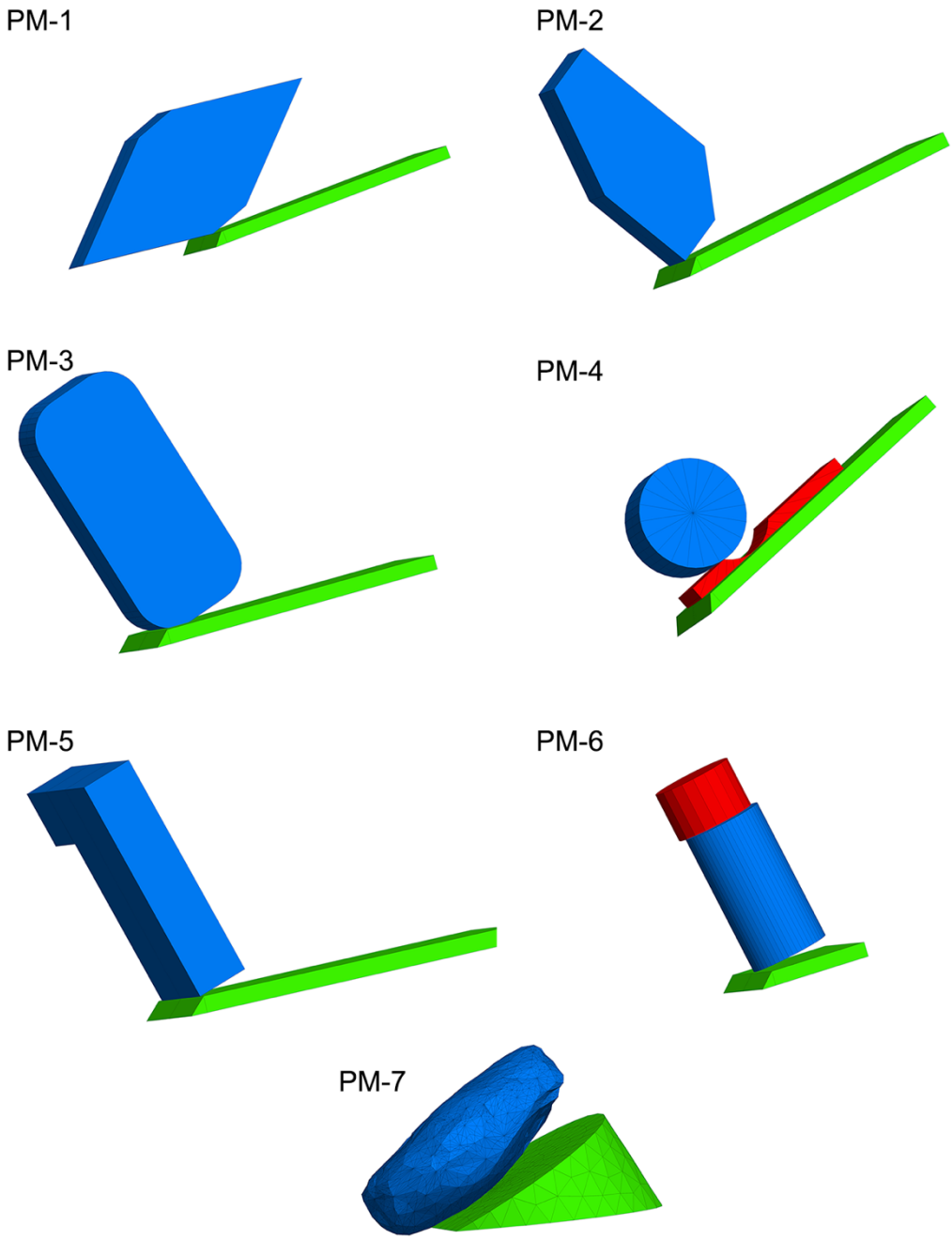

632

633 Fig. 20. Results for the numerical simulation of the tilt tests performed.
634

635

In these models, both the tilt table and the specimens were modelled as rigid blocks. The contact stiffnesses were set to k_n 650 GPa/s and k_s 150 GPa/s. The tilting rate was set slow enough to ensure that no inertial effect was produced so the test could be considered static. The results of these models are presented in Table 3, where the maximum difference observed between results obtained using various methods is indicated.

Table 3. Angles of critical toppling calculated by different methods and absolute maximum difference between results. Involved methods indicated in brackets.

Model	Angle of critical toppling (º)			Absolute max. difference (º)
	Experimental (E)	Analytical (A)	DEM (D)	
PM-1	20.3	20.32	20.1	0.22 (E-A)
PM-2	29.1	28.66	28.6	0.5 (E-N)
PM-3	10.6	10.01	10.0	0.6 (E-N)
PM-4	48.0	48.19	48.1	0.19 (E-A)
PM-5	12.1	11.88	11.9	0.22 (E-A)
PM-6	16.2	17.29	17.3	1.1 (E-N)
PM-7	30.6	31.39	31.3	0.79 (E-A)

The results obtained using the DEM models agree with those obtained by both the physical models and the analytical method, even in the cases where the centre of gravity is not located in the plane of symmetry, and the toppling involves complex movement not parallel to the tilting direction, as in the case of PM-6 (Fig. 21).

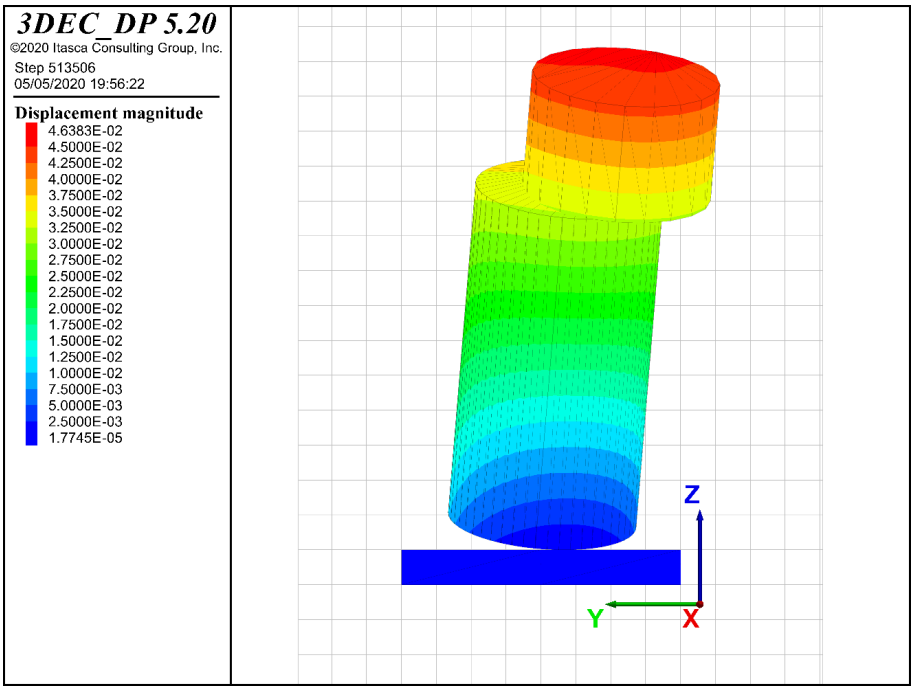

Fig. 21. 3DEC results of the tilt simulation on a rock + steel set with and upper cylinder uncentered r/2 to the left (PM-6). After the block starts to topple, its movement does not follow the tilting direction because the *cog* is not located in the symmetry plane as assumed in section 3.2.6

654 It is relevant to note that the DEM and the analytical approach match so closely here (and
655 in fact in general). This suggests that the errors observed in the experimental results are a
656 largely a function of limitations in the "manufacturing" processes used to make the
657 various specimens.
658 The critical angle in models with complex geometries (PM-7) measured by the three
659 methods were also similar, confirming the validity of both the experimental and the
660 analytical approaches. This model (Fig. 22) presents both an asymmetrical geometry and
661 an irregular base shape, resulting in complex movement after destabilization.
662

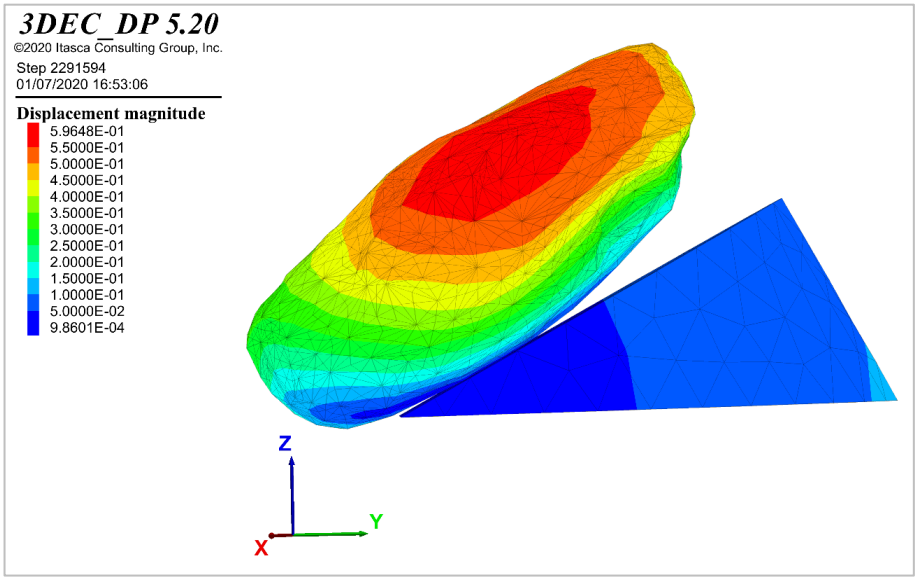

663

664 Fig. 22. Displacement magnitude after tilt-test of PM-7 calculated by 3DEC.

665

666 **5. Discussion**

667

668 It is not difficult in nature to find rock blocks or groups of blocks that could potentially
669 become unstable due to toppling. In some case, these blocks are irregular enough so as to
670 be considered heritage or part of natural parks, so they are protected (Fig. 23). On the
671 other hand, the instability of some other less aesthetically appealing rock blocks may
672 jeopardize infrastructure or even people, lives and properties. In any of these cases, it is
673 important to be able to analyze the stability of these blocks under different conditions
674 such that appropriate protective measures can be defined.
675

Although some approaches were developed in the past to compute the stability of blocks against toppling, in many cases, and specifically those corresponding to complex geometry blocks, it was indeed difficult to accurately compute stability against toppling. Recent advances in theoretical stability analysis based on idealized geometries (rounded corners, concave or convex surfaces) have contributed to a better understanding of toppling phenomena. The methodology or group of approaches presented here based on modern block geometry reconstruction methods, 3D printing of a block replica and testing of this replica using a tilt table, help to reproduce the potential instability phenomena of these blocks and to assess their degree of stability or instability.

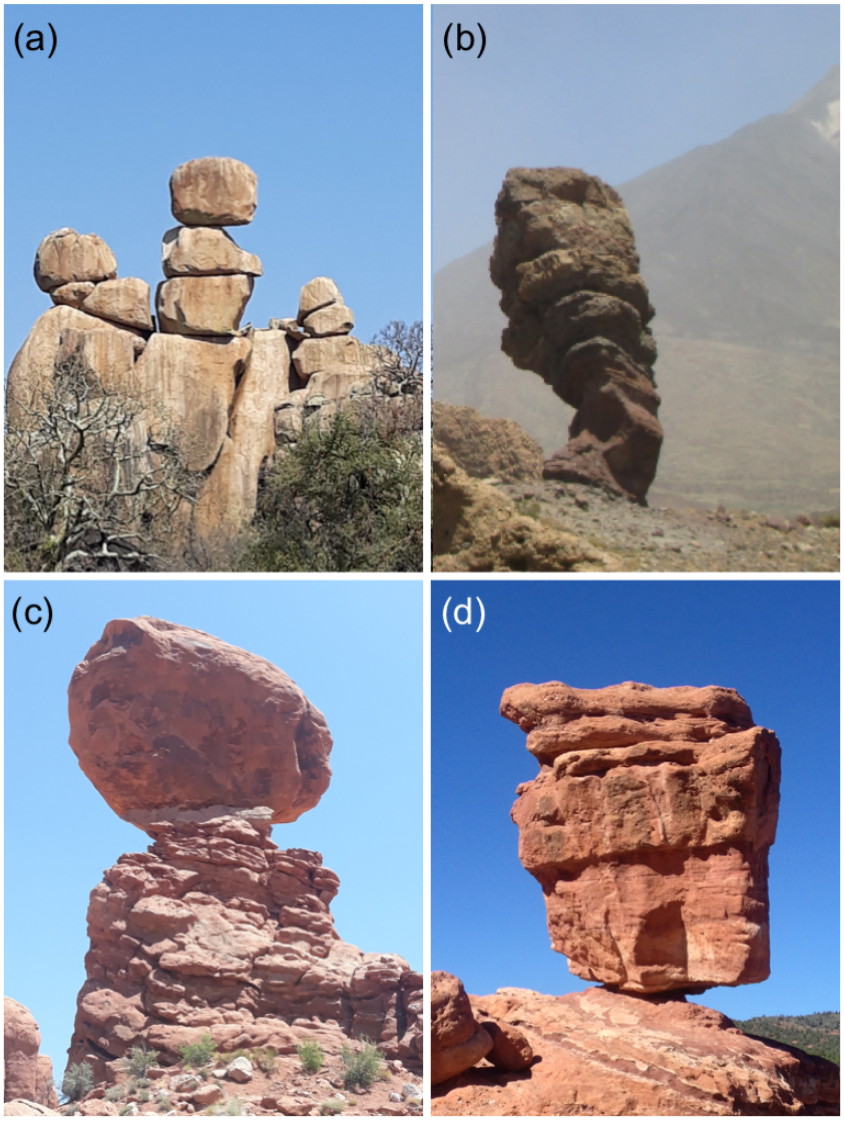

Figure 23. Balanced stones in different Natural Parks. (a) The three sisters balancing rocks, Matopos National Park, Matabeleland, Zimbabwe (b) Roque de García, basaltic horn at Teide National Park, Tenerife, Canary Islands, Spain (c) 3,500 t balanced rock, Arches National Park, Utah, USA and (d) 700 t balanced rock, the garden of gods, Colorado Springs, USA. Photos by the authors.

One notable limitation of the approach demonstrated in this study is the lack of knowledge of the geometry (concavity or concaveness and roughness) of the contact between the block and the surface where it rests and its actual frictional behavior. However, the proposed approach, in combination with detailed in-situ characterization and the application of analytical and numerical calculation techniques as illustrated in this document, has the potential to contribute to improved assessments of the stability of irregular rock blocks or boulders.

6. Conclusions

All over the world, and particularly in mountainous terrain in hot and temperate regions, rock blocks or boulders occur, and may exist in a state of marginal stability. In most of these cases, the potential instability of these blocks does not represent a hazard to human life or property. In some cases, however, it may be important to quantify block stability either due to an associated hazard, or due to its significance to the community or its natural landscape value.

Analyzing the stability of these blocks is not an easy task, primarily due to their complex geometry and because it is also difficult to characterize in sufficient detail all the features actually affecting their stability, including block geometry, geometry of the contact with the base surface, strength and deformability characteristics of this contact —of particular relevance when considering rough joints and infill material with non-negligible tensile strength—, and potential triggers such as water pressure and earthquake loading.

Recently developed remote-sensing tools, such as photogrammetry or LiDAR can be used in order to recover a rather accurate geometry of a block of interest as well as an approximate representation of the contact area (typically hidden). Based on the recovered 3D point cloud, a scaled version of the rock block or boulder can be 3D-printed, and its toppling behavior physically observed using a tilting platform, since toppling is exclusively dependent on the geometry of the potentially overturning object and the concavity of the base. This approach can be applied in combination with analytical or numerical techniques to study the mechanisms involved and to check physical testing results.

Acknowledgements

The last author acknowledges the Spanish Ministry of Universities for funding of his work in the project, awarded under Contract Reference No. RTI2018-093563-B-I00, partially financed by means of ERDF funds from the EU.

References

Akbarpour, T., Amini, M., Zamani, Z., 2012. Stability Analysis of Block Toppling Failures in Tunnels Portals of "Moshampa" Dam in Iran, in: Mechanics, K.S. for R. (Ed.), ISRM Regional Symposium - 7th Asian Rock Mechanics Symposium, 15-19 October, Seoul, Korea.

Al Mandalawi, M., You, G., Dahlhaus, P., Dowling, K., Sabry, M., 2019. Analysis of a Combined Circular--Toppling Slope Failure in an Open--Pit, in: Wasowski, J., Dijkstra, T. (Eds.), Recent Research on Engineering Geology and Geological Engineering. Springer International Publishing, Cham, pp. 10–30.

Alejano, L.R., Carranza-Torres, C., Giani, G., Arzúa, J., 2015. Study of the stability against toppling of rock blocks with rounded edges based on analytical and experimental approaches. Eng. Geol. 195, 172–184. https://doi.org/10.1016/j.enggeo.2015.05.030

Alejano, L.R., Castro-Filgueira, U., Pérez-Rey, I., Arzúa, J., 2017. Stability Analysis of an Over-tilted Slope in a Granite Quarry: The Role of Joint Spacing, in: Procedia Engineering. https://doi.org/10.1016/j.proeng.2017.05.197

Alejano, L.R., Ferrero, A.M., Ramírez-Oyanguren, P., Álvarez Fernández, M.I., 2011. Comparison of limit-equilibrium, numerical and physical models of wall slope stability. Int. J. Rock Mech. Min. Sci. 48, 16–26. https://doi.org/https://doi.org/10.1016/j.ijrmms.2010.06.013

Alejano, L.R., García-Cortés, S., García-Bastante, F., Martínez-Alegría, R., 2013. Study of a rockfall in a limy conglomerate canyon (Covarrubias, Burgos, N. Spain). Environ. Earth Sci. 70, 2703–2717. https://doi.org/10.1007/s12665-013-2327-x

Alejano, L.R., Gómez-Márquez, I., Martínez-Alegría, R., 2010a. Analysis of a complex toppling-circular slope failure. Eng. Geol. 114, 93–104. https://doi.org/10.1016/J.ENGGEO.2010.03.005

Alejano, L.R., Ordóñez, C., Armesto, J., Rivas, T., 2010b. Assessment of the instability hazard of a granite boulder. Nat. Hazards 53, 77–95. https://doi.org/10.1007/s11069-009-9413-0

Alejano, L.R., Veiga, M., Gómez-Márquez, I., Taboada, J., 2012. Stability of granite drystone masonry retaining walls: II. Relevant parameters and analytical and numerical studies of real walls. Géotechnique 62, 1027–1040. https://doi.org/10.1680/geot.10.P.113

Amini, M., Ardestani, A., 2019. Stability analysis of the north-eastern slope of Daralou copper open pit mine against a secondary toppling failure. Eng. Geol. 249, 89–101. https://doi.org/https://doi.org/10.1016/j.enggeo.2018.12.022

Armesto, J., Ordóñez, C., Alejano, L.R., Arias, P., 2009. Terrestrial laser scanning used to determine the geometry of a granite boulder for stability analysis purposes. Geomorphology 106, 271–277. https://doi.org/https://doi.org/10.1016/j.geomorph.2008.11.005

Ashby, J.P., 1971. Sliding and toppling modes of failure in models and jointed rock slopes (MSc thesis). London University - Imperial College (London).

Bader, C., Kolb, D., Weaver, J.C., Sharma, S., Hosny, A., Costa, J., Oxman, N., 2018. Making data matter: Voxel printing for the digital fabrication of data across scales and domains. Sci. Adv. 4, eaas8652. https://doi.org/10.1126/sciadv.aas8652

Barton, N., 1971. A model study of the behaviour of steep excavated rock slopes. University of London (Imperial College of Science and Technology).

Bray, J.W., 1969. Seminar on toppling failure. London.

Bray, J.W., Goodman, R.E., 1981. The theory of base friction models. Int. J. Rock Mech. Min. Sci. Geomech. Abstr. 18, 453–468. https://doi.org/https://doi.org/10.1016/0148-9062(81)90510-6

Brideau, M.-A., Stead, D., 2010. Controls on Block Toppling Using a Three-Dimensional Distinct Element Approach. Rock Mech. Rock Eng. 43, 241–260. https://doi.org/10.1007/s00603-009-0052-2

Cai, J., Ju, N., Huang, R., Zheng, D., Zhao, W., Li, L., Huang, J., 2019. Mechanism of toppling and deformation in hard rock slope: a case of bank slope of Hydropower

786 Station, Qinghai Province, China. J. Mt. Sci. 16, 924–934.
787 https://doi.org/10.1007/s11629-018-5096-x

788 Christianson, M., Itoh, J., Nakaya, S., 1995. Seismic analysis of the 25 Stone Buddhas
789 Group at Hakone, Japan. 35th U.S. Symp. Rock Mech.

790 Cignoni, P., Callieri, M., Corsini, M., Dellepiane, M., Ganovelli, F., Ranzuglia, G.,
791 2008. MeshLab: an Open-Source Mesh Processing Tool, in: Scarano, V., Chiara,
792 R. De, Erra, U. (Eds.), Eurographics Italian Chapter Conference. The Eurographics
793 Association.
794 https://doi.org/10.2312/LocalChapterEvents/ItalChap/ItalianChapConf2008/129-
795 136

796 Cundall, A.P., 1971. A Computer Model for Simulating Progressive, Large-scale
797 Movement in Blocky Rock System, in: International Symposium on Rock
798 Fractures. Nancy, France, p. Paper II-8.

799 Cundall, P., 1971. A computer model for simulating progressive large scale movements
800 in blocky rock systems, in: ISRM International Symposium on Rock Fracture.
801 Nancy (France).

802 Domokos, G., Sipos, A.Á., Szabó, T., 2012. The Mechanics of Rocking Stones:
803 Equilibria on Separated Scales. Math. Geosci. 44, 71–89.
804 https://doi.org/10.1007/s11004-011-9378-x

805 Ferrero, A., Migliazza, M., Roncella, R., Segalini, A., 2011. Rock cliffs hazard analysis
806 based on remote geostructural surveys: The Campione del Garda case study (Lake
807 Garda, Northern Italy). Geomorphology 125, 457–471.
808 https://doi.org/https://doi.org/10.1016/j.geomorph.2010.10.009

809 Ferrero, A.M., Forlani, G., Roncella, R., Voyat, H.I., 2009. Advanced Geostructural
810 Survey Methods Applied to Rock Mass Characterization. Rock Mech. Rock Eng.
811 42, 631–665. https://doi.org/10.1007/s00603-008-0010-4

812 Girardeau-Montaut, D., 2018. CloudCompare.

813 Goodman, R., Bray, J., 1976. Toppling of rock slopes, in: Proceedings of the Specialty
814 Conference on Rock Engineering for Foundations and Slopes. Vol. 2.

815 Guo, S., Qi, S., Yang, G., Zhang, S., Saroglou, C., Guo, S., Qi, S., Yang, G., Zhang, S.,

816 Saroglou, C., 2017. An Analytical Solution for Block Toppling Failure of Rock
817 Slopes during an Earthquake. Appl. Sci. 7, 1008.
818 https://doi.org/10.3390/app7101008

819 Hencher, S.R., 2015. Practical Rock Mechanics. CRC Press (Taylor and Francis
820 Group), Boca Raton, FL.

821 Hoek, E., Bray, J., 1974. Rock Slope Engineering. Chapman & Hall.

822 Itasca Consulting Group, I., 2019. 3 Dimensional Distinct Element Code. 3DEC.

823 Lanaro, F., Jing, L., Stephansson, O., Barla, G., 1997. DEM modelling of laboratory
824 tests of block toppling. Int. J. rock Mech. Min. Sci. Geomech. Abstr. 34, 506–507.
825 https://doi.org/10.1016/s1365-1609(97)00116-0

826 Müller, L., 1968. New considerations of the Vaiont slide. Felsmechanik und
827 engenieurgeologie 6, 1–91.

828 Pérez-Rey, I., Alejano, L.R., Riquelme, A., González-deSantos, L., 2019. Failure
829 mechanisms and stability analyses of granitic boulders focusing a case study in
830 Galicia (Spain). Int. J. Rock Mech. Min. Sci. 119, 58–71.
831 https://doi.org/https://doi.org/10.1016/j.ijrmms.2019.04.009

832 Pritchard, M.A., Savigny, K.W., 1990. Numerical modelling of toppling. Can. Geotech.
833 J. 27, 823–834. https://doi.org/10.1139/t90-095

834 Riquelme, A., Abellán, A., Tomás, R., Jaboyedoff, M., 2014. A new approach for semi-
835 automatic rock mass joints recognition from 3D point clouds. Comput. Geosci. 68,
836 38–52. https://doi.org/https://doi.org/10.1016/j.cageo.2014.03.014

837 Sagaseta, C., 1986. On the modes of instability of a rigid block on an inclined plane.
838 Rock Mech. Rock Eng. 19, 261–266. https://doi.org/10.1007/BF01039998

839 Shi, B., Anooshehpoor, A., Zeng, Y., Brune, J.N., 1996. Rocking and overturning of
840 precariously balanced rocks by earthquakes. Bull. Seismol. Soc. Am. 86, 1364–
841 1371.

842 St. John, C.M., 1972. Numerical and observational methods of determining the
843 behaviour of rock slopes in opencast mines. University of London - Imperial
844 College of Science and Technology.

Terzaghi, K., 1962. Stability of steep slopes on hard unweathered rock. Géotechnique 12, 251–270.

Tu, X., Dai, F., Lu, X., Zhong, H., 2007. Toppling and stabilization of the intake slope for the Fengtan Hydropower Station enlargement project, Mid-South China. Eng. Geol. 91, 152–167. https://doi.org/https://doi.org/10.1016/j.enggeo.2007.01.009

Vann, J.D., Olaiz, A.H., Morgan, S., Zapata, C., 2019. A Practical Approach to a Reliability-Based Stability Evaluation of Precariously Balanced Granite Boulders, in: Proceedings of the 53rd U.S. Rock Mechanics/Geomechanics Symposium. ARMA, New York, USA.

Virtanen, J.P., Hyyppä, H., Kurkela, M., Vaaja, M., Alho, P., Hyyppä, J., 2014. Rapid Prototyping — A Tool for Presenting 3-Dimensional Digital Models Produced by Terrestrial Laser Scanning. Int. J. Geo-Information 3, 871–890.

Wyllie, D., Mah, C., 2004. Rock Slope Engineering, 4th ed. CRC Press (Taylor and Francis Group).

Yeung, M.R., Wong, K.L., 2007. Three-dimensional Kinematic Conditions For Toppling, in: 1st Canada - U.S. Rock Mechanics Symposium. American Rock Mechanics Association, Vancouver, Canada, p. 5.

Zábranová, E., Matyska, C., Stemberk, J., Málek, J., 2020. Eigenoscillations and Stability of Rocking Stones: The Case Study of “The Hus Pulpit” in The Central Bohemian Pluton. Pure Appl. Geophys. 177, 1907–1916. https://doi.org/10.1007/s00024-019-02296-z

Declaration of interests

☒ The authors declare that they have no known competing financial interests or personal relationships that could have appeared to influence the work reported in this paper.

☐The authors declare the following financial interests/personal relationships which may be considered as potential competing interests:

On behalf of the co-authors:

PEREZ REY IGNACIO - 77005536H

Firmado digitalmente por PEREZ REY IGNACIO - 77005536H
Fecha: 2020.07.20 23:35:12 +02'00'

Ignacio Pérez-Rey, PhD (corresponding author)
Researcher in rock mechanics
Laboratorio de Geotecnia, CEDEX (Madrid)

Laboratory physical modelling of block toppling instability by means of tilt tests

CRediT author statement

Ignacio Pérez-Rey: Conceptualization, Methodology, Writing original draft; **Mauro Muñiz-Menéndez:** Software, Validation; **Javier González:** Visualization, Investigation; **Federico Vagnon:** Investigation; **Gabriel Walton:** Formal analysis, Writing - Review & Editing; **Leandro R. Alejano:** Supervision, Funding acquisition.